Middle Miocene extension in the Gulf Extensional Province, Baja California: Evidence from the southern Sierra Juarez

Jeffrey Lee
M. Meghan Miller } *Department of Geology, Central Washington University, Ellensburg, Washington 98926*
Robert Crippen *Jet Propulsion Laboratory, California Institute of Technology, 4800 Oak Grove Drive, Pasadena, California 91109*
Bradley Hacker *Department of Geology, Stanford University, Stanford, California 93405*
Jorge Ledesma Vazquez *Facultad de Ciencias Marinas, Universidad Autónoma de Baja California, Ensenada, Baja California, México 22800*

ABSTRACT

New geologic mapping, structural studies, and geochronology of Miocene volcanic and sedimentary rocks in the southern Sierra Juarez, Baja California, shed light on the extensional history of the Gulf Extensional Province prior to sea-floor spreading in the Gulf of California. The southern Sierra Juarez is underlain by lower–middle Miocene rocks including fluvial strata, intermediate composition volcanic deposits, basalt lava flows and cinder cones, and dacite pyroclastic deposits and lavas that nonconformably overlie the Cretaceous Peninsular Ranges batholith. The $^{40}Ar/^{39}Ar$ geochronology indicates that basaltic rocks are 16.90 ± 0.05 Ma and dacite pyroclastic deposits are between 16.69 ± 0.11 Ma and 15.98 ± 0.13 Ma. These strata were subsequently cut by two generations of faults. First generation faults comprise a dominant set of north-south–striking, west-dipping normal faults, a secondary set of north-south–striking, east-dipping normal faults, and a lesser set of variably oriented strike-slip faults. All three fault sets are temporally and spatially related and were produced by east-west extension. The dominant west-dipping faults, which are antithetic to and oblique to the east-dipping Main Gulf Escarpment, may have been a precursor or an early phase accommodation zone along the escarpment. West-dipping normal faults are cut by a 10.96 ± 0.05 Ma dacite hypabyssal intrusion, thus bracketing the age of east-west extension between 15.98 ± 0.13 Ma and 10.96 ± 0.05 Ma. Hence, this faulting event clearly indicates a period of extension that predates the onset of oceanic rifting and even predates other dated Miocene extension within Baja California. Second generation faults, which are comprised of east-west–striking strike-slip faults that cut first generation faults and associated northwest-striking, northeast-dipping normal faults, may be related to early development of the Transpeninsular Strike-slip Province.

Global plate reconstructions suggest that transtensional motion between the North American and Pacific plates along the western margin of Baja California began during middle Miocene time, coeval with east-west extension in the southern Sierra Juarez. This observation supports a hypothesis that middle Miocene transtensional plate motion was partitioned into two components: a strike-slip component parallel to active faults along the western offshore margin of Baja California, and an extensional component normal to the margin, but located in what is now the Gulf Extensional Province. Hence, the onset of extension within the circum-gulf region was in response to plate boundary processes.

INTRODUCTION

Baja California, Mexico, lies within a unique and complex plate tectonic setting, where the peninsula has been transferred from the North American plate to the Pacific plate during late Neogene time (Fig. 1). The peninsula is currently riding northwestward on the Pacific plate parallel to transform faults that define much of the plate boundary. Continental crust surrounding the Gulf of California records the transition from subduction to transform-dominated rifting. Extension is an important component in the tectonic development of this transform plate boundary, yet the causal relationship between extension and plate-boundary evolution is poorly understood and the subject of debate.

Early tectonic models proposed initiation of oceanic rifting in the Gulf of California at 5–4 Ma, accompanied by the apparently instantaneous transfer of Baja California from the North American plate to the Pacific plate and the translation of Baja California northward at plate boundary rates (Larson et al., 1968; Atwater, 1970; Moore and Curray, 1982). This interpretation is supported by NUVEL-1 (DeMets et al., 1990), which suggests oceanic rifting was initiated at 4.5 Ma. Geophysical, sedimentary, structural, and geochronologic evidence from the circum-gulf region, however, point to a period of middle–late Miocene (ca. 16–5 Ma) "proto-gulf" extension prior to the onset of sea-floor spreading (e.g., Karig and Jensky, 1972; Ingle, 1973, 1974; Angelier et al., 1981; Curray et al., 1982; Dokka and Merriam, 1982; Stock and Hodges, 1990; Lee and Miller, 1994).

Early workers attributed this period of proto-gulf extension to a back-arc setting (Karig and Jensky, 1972), although more precise dating indicates that the cessation of subduction occurred prior to the onset of extension (Mammerickx and Klitgord, 1982; Lonsdale, 1991; Stock and Hodges, 1990; Lee and Miller, 1994). Some have proposed that the proto-gulf period of extension accommodated Pacific–North American displacement perpendicular to preexisting/active strike-slip faults along the western margin of Baja California (Spencer and

GSA Bulletin; May 1996; v. 108; no. 5; p. 505–525; 14 figures; 3 tables.

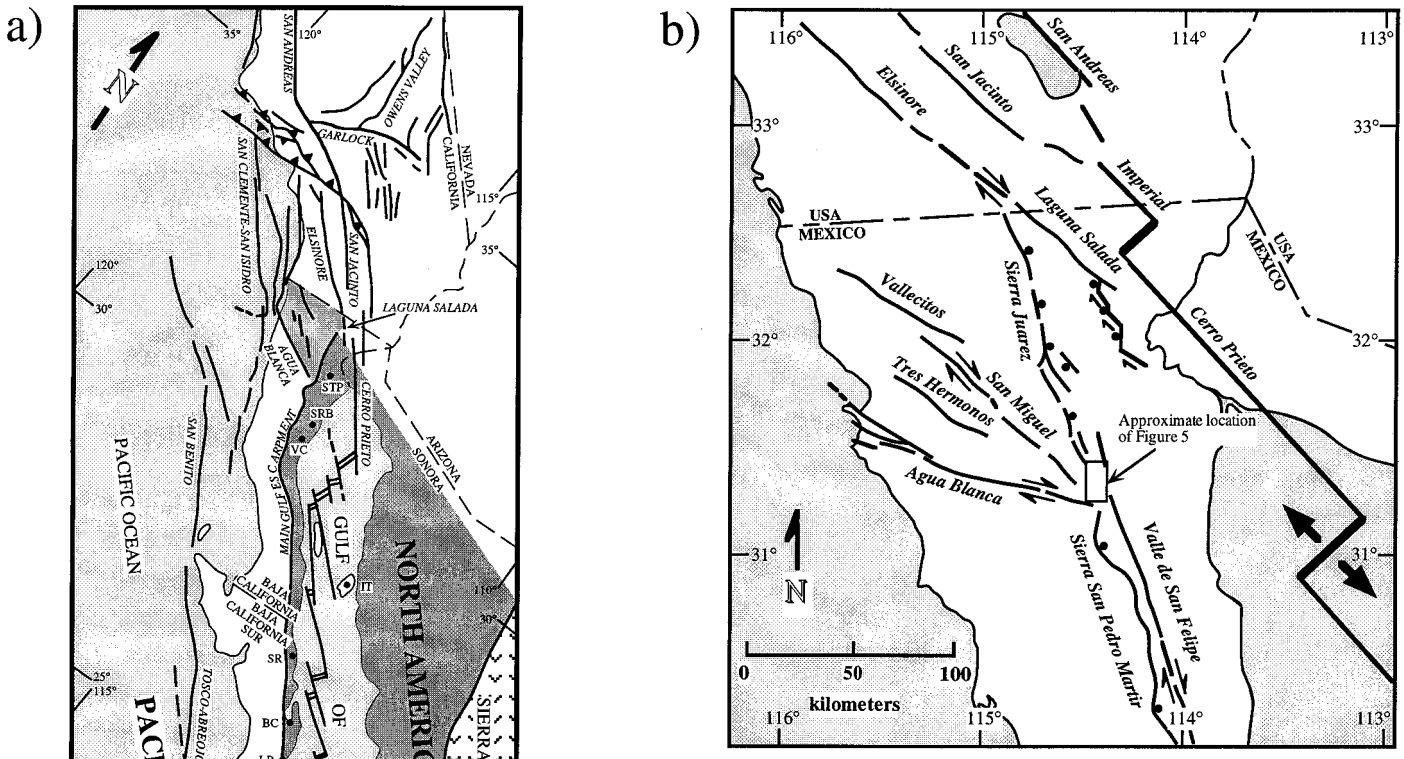

Figure 1. (a) Modern tectonic setting of the Pacific–North American plate boundary in southern California, the Baja California peninsula, and the Gulf of California. Gulf Extensional Province is shown in dark shade and Transpeninsular Strike-slip Province is shown in medium shade. Active and suspected faults that accommodate components of plate motion are shown; some fault names are given in italics. Abbreviations for areas discussed in text: BC, Bahia Concepcion; IT, Isla Tiburon; LP, La Paz; LR, Loreto; SR, Santa Rosalia; SRB, Santa Rosa Basin; STP, Sierra Las Tinaja and Sierra Las Pintas region; VC, Valle Chico. (b) Tectonic setting of the northern part of Baja California showing major active or recently active faults and location of study area.

Normark, 1979; Hausback, 1984; Stock and Hodges, 1989). Others, noting continuity, common fault geometry, and parallel extension direction with the southern Basin and Range Province, focus on a common origin (Gastil, 1968; Dokka and Merriam, 1982; Curray and Moore, 1984; Henry, 1989; Henry and Aranda-Gomez, 1992). A number of tectonic models have been proposed for the origin of the Basin and Range Province including: (1) distributed shear related to the onset of transform motion along the Pacific–North American plate boundary (Atwater, 1970), (2) migration of Mendocino triple junction (Ingersoll, 1982; Glazner and Bartley, 1984), (3) a decrease in plate convergence rates (Engebretson et al., 1984; Stock and Molnar, 1988), (4) change in plate motions (Pollitz, 1988; Stock and Hodges, 1989), (5) steepening and/or removal of the Laramide slab (Atwater, 1989), and (6) gravitational collapse of overthickened crust (Coney and Harms, 1984; Wernicke et al., 1987).

Global plate reconstructions for Baja California indicate a middle–late Miocene transition from subduction to transform plate motion (Stock and Molnar, 1988). In this scenario, Pacific–North American relative plate motion changed from parallel to oblique (transtensional) during middle Miocene time. Because there was no component of extension along the western margin of Baja California (Spencer and Normark, 1979; Hausback, 1984; Lonsdale, 1991), it has been suggested that plate boundary slip was partitioned into two components (Hausback, 1984; Stock and Hodges, 1989): one parallel to strike-slip faults along the western margin of Baja California (i.e., the San Benito and Tosco-Abreojos faults) and the other orthogonal to the margin along normal faults located in the Gulf Extensional Province. The partitioning of plate boundary slip, in effect, isolated Baja California between the Pacific plate to the west and the North American plate to the east. The location of middle–late Miocene extension, far inland from the plate margin, is suggested to result from a thermally weakened, recently active volcanic arc (Hausback, 1984; Stock and Hodges, 1989). Precise time constraints on the change in relative plate motion and onset of extension, however, are not known. On the basis of global plate reconstructions, transtension along the plate boundary was initiated as early as 15–9 Ma

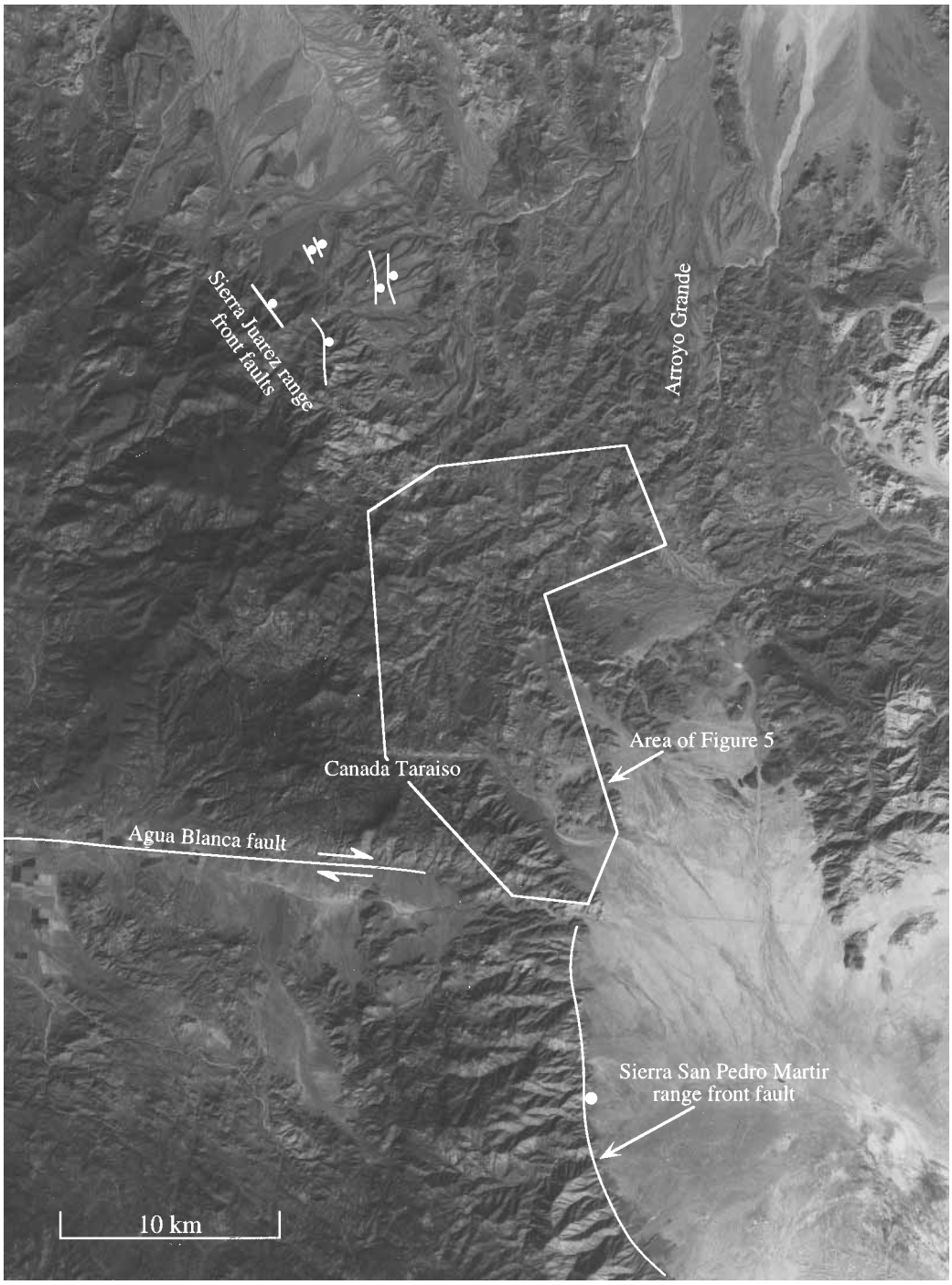

Figure 2. SPOT image of southeastern Sierra Juarez, northeastern Baja California, Mexico. Major geomorphically defined faults, drainages, and location of study area are shown.

and continued until 7–5 Ma (Stock and Hodges, 1989). A fixed hotspot reference frame model, however, indicates transtensional plate motion began at least as early as 17 Ma (Engebretson et al., 1985).

Humphreys and Weldon (1991), on the other hand, argue that because Pacific–North American plate motion since 5–4 Ma cannot account for the minimum geologic separation of Baja California from central Mexico, the onset of proto-gulf deformation is a direct consequence of increased activity along the proto–San Andreas fault system at 17 Ma. Humphreys and Weldon's (1991) synthesis of geologic relations, combined with plate motion constraints, points to the interplay of extension and transform motion during the late Neogene, but emphasizes dextral transform motion in the proto-gulf region.

With some exceptions (e.g., Henry, 1989; Stock and Hodges, 1990; Lewis, 1994), the paucity of detailed geologic and geochronologic constraints on extension in Baja Cali-

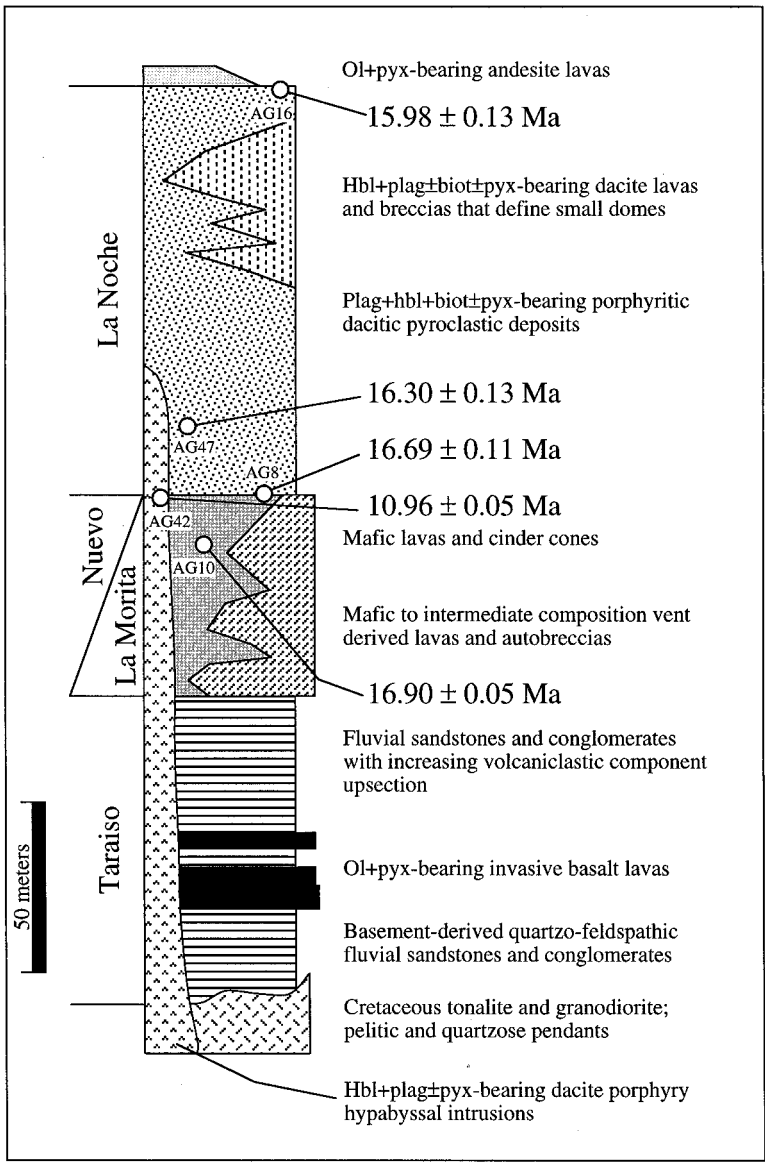

Figure 3. Simplified stratigraphic column for the Arroyo Grande area, southern Sierra Juarez. Approximate stratigraphic position of geochronology samples are shown.

fornia and mainland Mexico hinder rigorous understanding of the timing and geometry of extension and its role in proto-gulf and gulf evolution. Further refinement of our understanding of this rapidly evolving plate boundary hinges on characterizing the nature and timing of extension. In order to address questions about the causes of early continental extension, we report results of geologic mapping, and structural and geochronologic studies of volcanic rocks and normal faulting in the southern Sierra Juarez, Baja California.

GEOLOGY OF THE SOUTHERN SIERRA JUAREZ

Regional Setting

Baja California comprises three structural provinces: (1) the Gulf Extensional Province, which is present along the eastern margin of Baja California, (2) the Transpeninsular Strike-slip Province, which encompasses the northwestern part of Baja California, and (3) the stable central and southern peninsula, which includes most of the remainder of the peninsula (Fig. 1). The Gulf Extensional Province is bounded to the west by the Main Gulf Escarpment, a north-south–striking, steeply east-dipping normal fault, and to the northeast by the Sierra Madre Occidental (Stewart, 1978; Henry and Aranda-Gomez, 1992), a relatively unextended high plateau of predominantly flat-lying Oligocene–lower Miocene rhyolite volcanic rocks (McDowell and Keizer, 1977; Fig. 1). The Gulf Extensional Province is characterized by basin and range–type topography and lies within a broad region of Cenozoic extension in western North America, which includes parts of the southwestern United States and northern Mexico east of the Sierra Madre Occidental (Stewart, 1978; Henry, 1989; Henry and Aranda-Gomez, 1992). The province is underlain by Cretaceous granodiorite and tonalite of the Peninsular Ranges batholith that intruded Paleozoic and Mesozoic oceanic, arc, and continent margin rocks. The uplifted crystalline rocks are regionally overlain by Cenozoic sedimentary and volcanic rocks (Minch, 1979; Gastil et al., 1975, 1981).

Our study area is located along the Main Gulf Escarpment, on the western edge of the Gulf Extensional Province. It is centered on Arroyo Grande in the southeastern Sierra Juarez (Figs. 1b, 2, and 5 below), where several currently active or recently active faults converge. These include the east-dipping Main Gulf Escarpment defined by the Sierra San Pedro Martir to the south and the central and northern Sierra Juarez to the north, the east-west– to northwest-striking, right-lateral Agua Blanca and Vallecitos–San Miguel fault systems, and the north-northwest–striking, oblique-slip Valle de San Felipe fault to the southeast (Figs. 1b and 2).

Methods of Study

Geologic mapping on a 1:25 000-scale topographic base and standard stratigraphic and structural field studies reported here were augmented with 1:50 000-scale aerial photograph and remote sensing studies, and $^{40}Ar/^{39}Ar$ geochronology. Landsat Thematic Mapper (Landsat TM) and Système Probatoire d'Observation de la Terre (SPOT) imagery provided a reconnaissance data base that guided our field studies. Geochronology was used to date the Tertiary volcanic sequence described below and to constrain the age of deformation in the area. The techniques we employed are briefly outlined here.

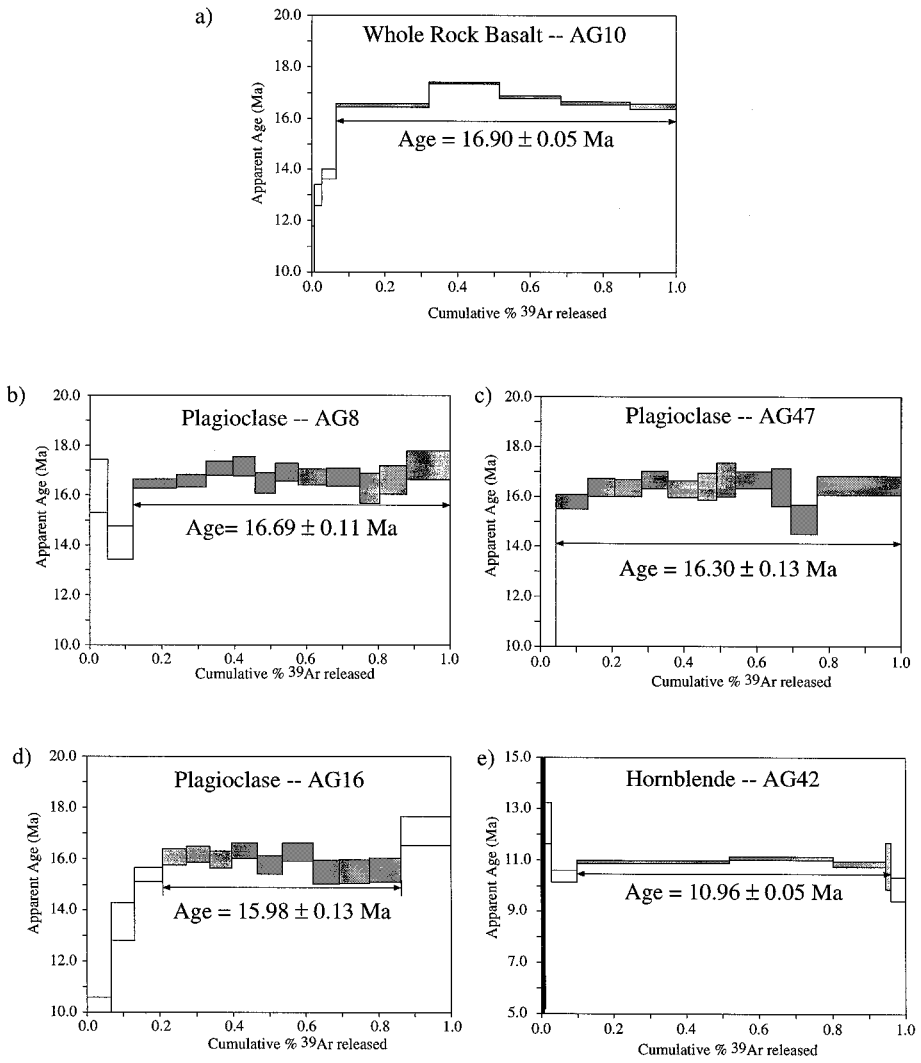

Figure 4. $^{40}Ar/^{39}Ar$ age spectra from the sequence of volcanic rocks and hypabyssal intrusion. (a) Sample AG10 is a whole rock basalt from near the top of the Nuevo mafic volcanic rocks. (b) Sample AG8 is a plagioclase separate from a clast at the base of the La Noche dacite. (c) Sample AG47 is a plagioclase separate from a tuff in the middle of the La Noche dacite. (d) Sample AG16 is a plagioclase separate from a lava flow at the top of the La Noche dacite. (e) Sample AG42 is a hornblende separate from a dacite porphyry hypabyssal intrusion. Shaded steps are those used in determining the weighted mean plateau age. See text for details.

Image Processing and Interpretation. Landsat TM and SPOT panchromatic images were used to optimize the depiction of geomorphic and structural features and lithologic contrasts. The SPOT images were enhanced using a high-pass 5 × 5 box filter. The high-pass output was then stretched (usually by a factor of 2) and added to the original data prior to a linear contrast enhancement. The Landsat TM images were processed by band ratioing, using the combination 3/1 in blue, 5/4 in green, and 5/7 in red. This ratio combination provides maximum differentiation of the spectral contrasts that result from lithologic variation (Crippen, 1989a). Atmospheric corrections are critical in the ratioing process and are derived by an empirical "iterative ratioing" procedure (Crippen, in press a). The 3/1, 5/4, and 5/7 ratios are generally correlated with variations in ferric iron, ferrous iron, and hydroxyl minerals, respectively. The 5/4 also varies with desert varnish, and the 5/7 also varies with carbonate and vegetation. Scan-line noise is common in Landsat TM ratio images and was suppressed by a filtering routine (Crippen, 1989b).

Topographic shading in the imagery is important both for delineating structural features and for discriminating lithology via their geomorphic expression. A band-average image was used for maximum clarity and was high-pass enhanced to sharpen detail. Then this image was merged with the ratios by image multiplication, after adjustment of the relative coefficients of variation, which control the prominence of each image in the merger (Crippen, in press b). Typically, the results display excellent spectral discrimination of lithology as chromatic contrasts and detailed geomorphic expression as variations in image intensity. These images are particularly well suited to neotectonic studies in northern Baja California, where young faulting is expressed both by geomorphology and by lithologic discontinuities, and the relatively arid climate minimizes interference by vegetation.

The Arroyo Grande area was chosen because interpretation of the imagery indicated that the study area contained Tertiary volcanic rocks that would likely yield age constraints relative to deformation, occupied a little-studied transition between numerous modern and ancient structural domains, and was characterized by the absence of a geomorphically well-defined range front fault along the Main Gulf Escarpment (Fig. 2). Beyond the general distribution of map units known from earlier studies (e.g., Gastil et al., 1975), the wealth of geomorphic and lithologic information depicted by the images delineates major faults and volcanic centers. This information was used to guide field studies and provide first-order constraints beyond the limits of our map area.

$^{40}Ar/^{39}Ar$ Geochronology. Age determinations for volcanic units come from $^{40}Ar/^{39}Ar$ analyses of five samples. The samples came from the thick sequence of Nuevo mafic volcanic rocks, the La Noche dacite, and a cross-cutting hypabyssal dike described below (Fig. 3). These samples were selected to provide age constraints on eruption of the volcanic rocks, emplacement of intrusions, and motion along faults (see "Structural Chronology" below).

Mineral separates were obtained using magnetic separatory methods, heavy liquids (hornblende only), washing in dilute HCl (when needed), and hand picking to >99% purity. Samples were wrapped in aluminum foil, placed in evacuated quartz vials with flux monitor Taylor Creek sanidine (assumed age = 27.92 Ma), and irradiated for 8 hr at the TRIGA reactor, Oregon State University. Flux monitors were placed at

1.37 cm intervals in each quartz vial to determine flux gradients. Samples were analyzed at Stanford University by step heating in a Ta crucible and replaceable Mo liner within a double-vacuum Staudacher-type resistance furnace in cycles with 10 min of heating, 5 min of gettering with hot TiZrAl, and 6–12 min of static analysis in a MAP-216 spectrometer. Temperatures were monitored with a tungsten-rhenium thermocouple to ±5 °C. The extraction line blank was typically 1×10^{-15} moles ^{40}Ar at 800 °C. See Hacker (1993) for method of calculating isotopic abundances, corrections, and uncertainties. Because the trapped $^{40}Ar/^{36}Ar$ ratio of each sample, determined by a York regression of an inverse isochron plot ($^{39}Ar/^{40}Ar$ versus $^{36}Ar/^{40}Ar$), is not significantly different from the atmospheric ratio of 295.5, we report weighted mean plateau ages (shaded steps in Fig. 4). Results of isotopic analyses are listed in Table 1.

TABLE 1. ISOTOPIC ANALYSES OF DATED SAMPLES

Temperature (°C)	^{40}Ar (mol)†	$^{40}Ar/^{39}Ar$	$^{37}Ar/^{39}Ar$	$^{36}Ar/^{39}Ar$	K/Ca	$\Sigma^{39}Ar_K$§	$^{40}Ar^{*}$#	Age ± 1σ (Ma)
Sample: AG42 hornblende (J = 0.0023450)								
Total fusion age (TFA) = 10.60 ± 0.15 Ma								
Weighted mean plateau age (WMPA) = 10.96 ± 0.05 Ma								
Steps used: 1150 – 1210, or 82% $\Sigma^{39}Ar$								
Inverse isochron age = 11.04 ± 0.13 Ma (MSWD = 0.94; $^{40}Ar/^{36}Ar$ = 292.7 ± 4.0)								
700	2.1e–15	–282.7204	35.8293	1.7782	0.013	0.000	–1.119	–1962.1 ± 509.6
800	4.7e–14	–1.4491	8.0590	2.0059	0.061	0.001	–0.002	–6.14 ± 63.76
850	7.8e–14	–11.5717	10.2254	4.9199	0.048	0.002	–0.008	–49.63 ± 128.75
900	3.5e–14	–6.3712	6.4026	1.0504	0.076	0.004	–0.021	–27.16 ± 16.53
950	1.1e–14	6.2516	6.5356	0.2602	0.075	0.006	0.075	26.25 ± 7.85
1000	1.6e–14	1.4781	9.9320	0.5396	0.049	0.008	0.009	6.24 ± 13.39
1050	1.3e–14	2.5895	13.9786	0.2446	0.035	0.011	0.035	10.92 ± 5.74
1100	1.7e–14	2.9506	17.4786	0.0495	0.028	0.028	0.181	12.44 ± 0.81
1125	3.9e–14	2.4562	18.8408	0.0269	0.026	0.099	0.274	10.36 ± 0.23
1150	1.3e–13	2.5886	19.1227	0.0138	0.025	0.518	0.503	10.92 ± 0.06
1165	7.0e–14	2.6227	19.3862	0.0101	0.025	0.802	0.649	11.06 ± 0.07
1185	3.8e–14	2.5709	19.5847	0.0114	0.025	0.946	0.588	10.84 ± 0.12
1210	1.6e–14	2.5521	19.3338	0.0557	0.025	0.960	0.145	10.76 ± 0.91
1300	3.8e–14	2.3403	21.8948	0.0508	0.022	1.000	0.149	9.87 ± 0.46
Sample: AG16 plagioclase (J = 0.0023660)								
Total fusion age (TFA) = 15.45 ± 0.15 Ma								
Weighted mean plateau age (WMPA) = 15.98 ± 0.13 Ma								
Steps used: 925 – 1300, or 65% $\Sigma^{39}Ar$								
Inverse isochron age = 16.13 ± 0.32 Ma (MSWD = 0.77; $^{40}Ar/^{36}Ar$ = 293.0 ± 5.0)								
700	5.2e–14	2.2704	2.7129	0.0783	0.18	0.066	0.090	9.66 ± 0.92
800	9.8e–14	3.1883	6.7102	0.1604	0.073	0.130	0.064	13.56 ± 0.74
875	1.8e–14	3.6188	11.3937	0.0166	0.043	0.208	0.474	15.38 ± 0.27
925	1.4e–14	3.7817	12.2353	0.0138	0.040	0.272	0.550	16.07 ± 0.33
975	1.5e–14	3.8046	12.2271	0.0153	0.040	0.337	0.516	16.17 ± 0.31
1015	1.5e–14	3.7567	12.2024	0.0183	0.040	0.396	0.457	15.96 ± 0.34
1060	1.6e–14	3.8379	12.1718	0.0157	0.040	0.467	0.510	16.31 ± 0.31
1100	1.6e–14	3.7086	12.3207	0.0156	0.039	0.536	0.505	15.76 ± 0.36
1150	2.2e–14	3.8250	12.2621	0.0190	0.040	0.619	0.451	16.25 ± 0.36
1190	1.1e–14	3.6409	11.9747	0.0081	0.041	0.691	0.718	15.47 ± 0.46
1250	2.2e–14	3.6473	11.9706	0.0203	0.041	0.775	0.418	15.50 ± 0.45
1300	3.5e–14	3.6606	11.9607	0.0354	0.041	0.862	0.277	15.56 ± 0.47
1400	4.2e–16	4.0216	11.9412	–0.0099	0.041	1.000	1.000	17.08 ± 0.57
Sample: AG47 plagioclase (J = 0.0023530)								
Total fusion age (TFA) = 15.64 ± 0.19 Ma								
Weighted mean plateau age (WMPA) = 16.30 ± 0.13 Ma								
Steps used: 900 – 1400, or 96% $\Sigma^{39}Ar$								
Inverse isochron age = 16.75 ± 0.20 Ma (MSWD = 0.29; $^{40}Ar/^{36}Ar$ = 288.7 ± 2.4)								
700	1.7e–13	–1.0008	4.0480	0.9522	0.12	0.019	–0.004	–4.25 ± 5.21
800	1.9e–13	1.1961	9.3614	0.8992	0.052	0.043	0.004	5.07 ± 3.55
900	3.6e–14	3.7358	12.7557	0.0349	0.038	0.132	0.285	15.79 ± 0.29
950	2.3e–14	3.8749	13.0876	0.0255	0.037	0.206	0.372	16.37 ± 0.37
1000	2.0e–14	3.8673	12.9616	0.0195	0.037	0.281	0.448	16.34 ± 0.34
1050	1.6e–14	3.9436	12.7736	0.0141	0.038	0.354	0.556	16.66 ± 0.35
1100	1.8e–14	3.8581	12.8829	0.0137	0.038	0.438	0.560	16.30 ± 0.33
1150	1.3e–14	3.8819	12.9055	0.0186	0.038	0.490	0.463	16.40 ± 0.54
1200	4.6e–15	3.9447	12.8085	–0.0003	0.038	0.542	1.400	16.67 ± 0.68
1200	1.6e–14	3.9446	12.5688	0.0074	0.039	0.642	0.771	16.67 ± 0.33
1250	1.9e–14	3.8748	12.3724	0.0294	0.039	0.696	0.333	16.37 ± 0.77
1300	3.6e–14	3.5680	12.3299	0.0455	0.039	0.768	0.221	15.08 ± 0.59
1400	3.2e–14	3.8918	13.0583	0.0056	0.037	1.000	0.864	16.44 ± 0.38

Sedimentary and Volcanic Stratigraphy, Related Hypabyssal Rocks

Middle Miocene and Older? Rocks. Cenozoic continental sedimentary and volcanic rocks regionally overlie the Cretaceous Peninsular Ranges batholith in northern Baja California along a widespread nonconformity that records unroofing of the batholith during latest Cretaceous or Paleogene time (Gastil et al., 1975; Minch, 1979). The oldest strata in the southeastern Sierra Juarez study area are probably early Miocene or only slightly older, because there is no pronounced stratigraphic break between the basal part of the sequence and rocks of that age. In the following descriptions, volcanic rock compositions are inferred from field observations and petrography and are confirmed by preliminary major and trace-element analyses (Lee, unpubl. data).

The basal unit, informally referred to as the Taraiso deposits (Fig 3), comprises thick-bedded, quartzofeldspathic, pebble- and cobble–bearing sandstone with locally well-developed foreset cross-stratification. Pebbles and cobbles consist of angular to subrounded granitic and metasedimentary clasts. Clast compositions near the base indicate derivation from the underlying granitic and tonalitic Cretaceous batholith and its metamorphic wall rock. Volcanic clasts are increasingly evident up-section, pointing to a developing volcanic source. The fluvial sandstone is interlayered with invasive olivine + pyroxene–bearing basalt flows that exhibit pillow structures and have been hydrothermally altered to palagonite at the top and base, suggesting interaction with wet fluvial sediments.

In the southern part of the map area, the Taraiso deposits are overlain by a poorly exposed, variably thick (as much as 150 m), diverse section of mafic to intermediate composition vent related deposits, informally referred to as the La Morita vent deposits (Fig. 3). These deposits include crystal-poor, olivine + plagioclase ± pyroxene–bearing basaltic to basaltic andesite cinder and block deposits, debris flows, autobreccias and lavas, and crystal-rich, hornblende + plagioclase ± pyroxene–bearing andesitic to dacitic lavas and autobreccias. These deposits commonly contain clots of olivine + pyroxene ± plagioclase crystals. The morphology of these deposits defines a small vent with a 0.7-km-wide depression. In the southern part of the map area, these deposits are overlain by the pyroclastic deposits of the La Noche dacite; to the north, these deposits thin and are overlain by ba-

TABLE 1. *(Continued)*

Temperature (°C)	^{40}Ar (mol)†	$^{40}Ar/^{39}Ar$	$^{37}Ar/^{39}Ar$	$^{36}Ar/^{39}Ar$	K/Ca	$\Sigma^{39}Ar_K$§	$^{40}Ar^{*\#}$	Age ± 1σ (Ma)
Sample: AG8 plagioclase (J = 0.0023630)								
Total fusion age (TFA) = 16.55 ± 0.14 Ma								
Weighted mean plateau age (WMPA) = 16.69 ± 0.11 Ma								
Steps used: 900 – 1400, or 88% $\Sigma^{39}Ar$								
Inverse isochron age = 16.77 ± 0.16 Ma (MSWD = 0.70; $^{40}Ar/^{36}Ar$ = 293.0 ± 3.7)								
700	4.8e–14	3.8546	3.7078	0.0876	0.13	0.050	0.131	16.36 ± 1.07
800	1.0e–13	3.3195	7.4562	0.1480	0.065	0.120	0.071	14.10 ± 0.66
900	2.3e–14	3.8782	10.5232	0.0097	0.046	0.240	0.657	16.46 ± 0.19
950	1.6e–14	3.9051	11.2415	0.0099	0.043	0.321	0.659	16.57 ± 0.25
1000	1.2e–14	4.0245	11.4337	0.0065	0.043	0.396	0.799	17.07 ± 0.29
1033	1.1e–14	4.0438	11.4567	0.0087	0.042	0.457	0.711	17.16 ± 0.39
1067	1.1e–14	3.8860	11.6580	0.0100	0.042	0.514	0.656	16.49 ± 0.42
1100	1.4e–14	3.9847	12.0236	0.0124	0.040	0.577	0.594	16.91 ± 0.36
1150	1.9e–14	3.9419	12.0893	0.0154	0.040	0.656	0.523	16.73 ± 0.32
1200	1.3e–14	3.9377	11.9346	0.0044	0.041	0.749	0.923	16.71 ± 0.36
1250	1.6e–14	3.8355	11.7000	0.0216	0.042	0.803	0.411	16.28 ± 0.61
1300	3.6e–14	3.9145	11.7713	0.0397	0.041	0.879	0.265	16.61 ± 0.57
1400	1.3e–14	4.0556	12.0854	0.0008	0.040	1.000	1.231	17.21 ± 0.58
Sample: AG10 whole rock basalt (J = 0.0023340)								
Total fusion age (TFA) = 16.41 ± 0.06 Ma								
Weighted mean plateau age (WMPA) = 16.90 ± 0.05 Ma								
Steps used: 900 – 1300, or 93% $\Sigma^{39}Ar$								
Inverse isochron age = 17.05 ± 0.25 Ma (MSWD = 46.68; $^{40}Ar/^{36}Ar$ = 288.4 ± 6.9)								
500	3.3e–14	–62.0603	8.9061	2.6556	0.055	0.000	–0.085	–282.28 ± 106.87
600	4.5e–14	2.2756	1.9180	0.2072	0.26	0.007	0.036	9.56 ± 2.22
700	2.9e–14	3.0994	1.3155	0.0311	0.37	0.027	0.254	13.00 ± 0.41
800	3.1e–14	3.2947	1.5506	0.0126	0.32	0.067	0.478	13.82 ± 0.19
900	2.8e–13	3.9348	1.5919	0.0192	0.31	0.322	0.415	16.49 ± 0.07
1000	1.1e–13	4.1469	1.7043	0.0033	0.29	0.515	0.832	17.38 ± 0.06
1100	8.8e–14	4.0131	0.9935	0.0021	0.49	0.684	0.882	16.82 ± 0.07
1200	1.0e–13	3.9584	1.9452	0.0031	0.25	0.874	0.837	16.59 ± 0.07
1300	9.3e–14	3.9301	13.5046	0.0124	0.036	1.000	0.602	16.47 ± 0.11

Note: MSWD: mean sum of weighted deviates; expresses the goodness of fit of the isochron.
†^{40}Ar (mol): ^{40}Ar moles corrected for blank and reactor-produced ^{40}Ar.
§$\Sigma^{39}Ar$: cumulative ^{39}Ar released.
#$^{40}Ar^*$: radiogenic fraction of ^{40}Ar.

salt lavas and cinder deposits of the Nuevo mafic volcanic rocks (Figs. 3 and 5).

In the northern part of the map area, the Taraiso deposits are overlain by a thick (as much as 168 m) section of olivine + pyroxene ± plagioclase–bearing basalt lava flows, cinder deposits, and small cinder cones, informally assigned to the Nuevo mafic volcanic rocks (Fig. 3). Flow foliations in lavas are locally well developed and defined by platy partings, but, where absent, vertical or radial fractures are typically developed. Granitic debris entrained in several flows ranges in size from rounded tonalite and granodiorite cobbles and small boulders to coarse crystals of quartz and feldspar. Feldspar crystals commonly show evidence of resorption.

Interbedded with the basalt lavas are red to orange, typically well-bedded, calcite-cemented cinder deposits. These deposits consist of small (as much as 1 cm across) rounded fragments of scoria, vesicular basaltic bombs as much as 1.0 m across, and granitic debris. Scarce cinder cones are cross-cut by radially distributed basalt dikes. Also, interbedded with the Nuevo mafic volcanic rocks are lesser, basalt-derived, volcaniclastic fluvial deposits and dacitic lapilli–bearing mudflows.

A concentrate of the nonmagnetic fraction of a whole rock sample from an olivine + pyroxene basalt lava flow (AG10) within the Nuevo mafic volcanic rocks (Figs. 3 and 5) yields an $^{40}Ar/^{39}Ar$ age of 16.90 ± 0.05 Ma (Fig. 4). This date provides an age for the upper part of the Nuevo mafic volcanic rocks.

A sequence of pyroclastic deposits, informally assigned to the La Noche dacite, overlies the Nuevo mafic volcanic rocks to the north and the La Morita vent deposits to the south (Figs. 3 and 5). These deposits are dominated by red, brown, tan, and gray, ledge- to cliff-forming, generally conformable, variably thick (as much as 250 m) massive to thick-bedded debris flows (lahars) comprised of angular, poorly sorted, matrix supported clasts. Clast sizes are variable and as much as several meters across. Clast populations are dominated by crystal-rich, plagioclase + hornblende ± biotite ± pyroxene–bearing porphyritic dacite lava and also include lesser basaltic, granitic, and metasedimentary rocks. Interbedded with these deposits are lesser crystal-rich plagioclase + hornblende ± biotite–bearing unwelded to partially welded dacitic to andesitic tuffs, lithic tuffs, lapilli tuffs, tuffaceous debris flows, ash flows, and mud flows. Individual ash flows are as much as 10 m thick; pumice fragments are generally unwelded and as much as 30 cm across.

The coarse pyroclastic debris flows of the La Noche dacite were likely deposited on at least a gentle slope. Nevertheless, the overall dip of the unit is similar to that of other stratigraphic units and is thus primarily attributed to structural deformation. To the northeast, the La Noche dacite interfingers with crystal-rich, hornblende + plagioclase ± biotite ± pyroxene dacite lava and breccia that define small domes. The $^{40}Ar/^{39}Ar$ geochronology of plagioclase from a debris flow clast at the bottom of La Noche dacite, a tuffaceous unit in the middle, and a lava flow at the top yields ages of 16.69 ± 0.11, 16.30 ± 0.13, and 15.98 ± 0.13 Ma, respectively (Figs. 3, 4, and 5). These indicate that deposition of the La Noche dacite pyroclastic sequence occurred between 16.69 ± 0.11 Ma and 15.98 ± 0.13 Ma. Locally, olivine + pyroxene andesite lavas cap the La Noche dacite (Fig. 3).

The volcanic and sedimentary section of basalt flows and cinder deposits, and dacitic pyroclastic deposits, is probably correlative to regionally widespread lower and middle Miocene arc volcanic and fluvial sedimentary deposits (Dorsey and Burns, 1994; Stock, 1989; Gastil et al., 1979) dated by the K/Ar method at between 15.0 ± 0.7 Ma and 21.6 ± 5.5 Ma in the central Sierra Juarez (Gastil et al., 1975, 1979).

Upper Middle Miocene Hypabyssal Rocks. Strongly altered olivine + pyroxene–bearing basalt dikes and olivine + hornblende + plagioclase–bearing intermediate dikes of unknown absolute age are younger than the volcanic section described above. Some of these dikes have intruded along first generation faults indicating that they are syn- to posttectonic with respect to movement along these faults.

Crystal-poor, hornblende + plagioclase ± pyroxene dacite porphyry vents and hypabyssal intrusions, with rare granitic inclusions, cut across the lower–middle Miocene volcanic section and first generation faults (Figs. 3 and 5). Borders of the small intrusions possess quench textures, whereas the cores have a fine grained, sugary texture.

LEGEND
Sedimentary and Volcanic Rocks
alluvium, colluvium, and landslides, undifferentiated
older alluvium, fan, and, fluvial deposits, undifferentiated
andesite lava flows
dacite pyroclastic debris flows
Late Miocene
Plio.-Quat.
Quat.
N
A
A'
Arroyo Grande
AG47
AG42
AG10
AG8
AG16
31°27.5'
115°30'
31°25'
115°27.5'

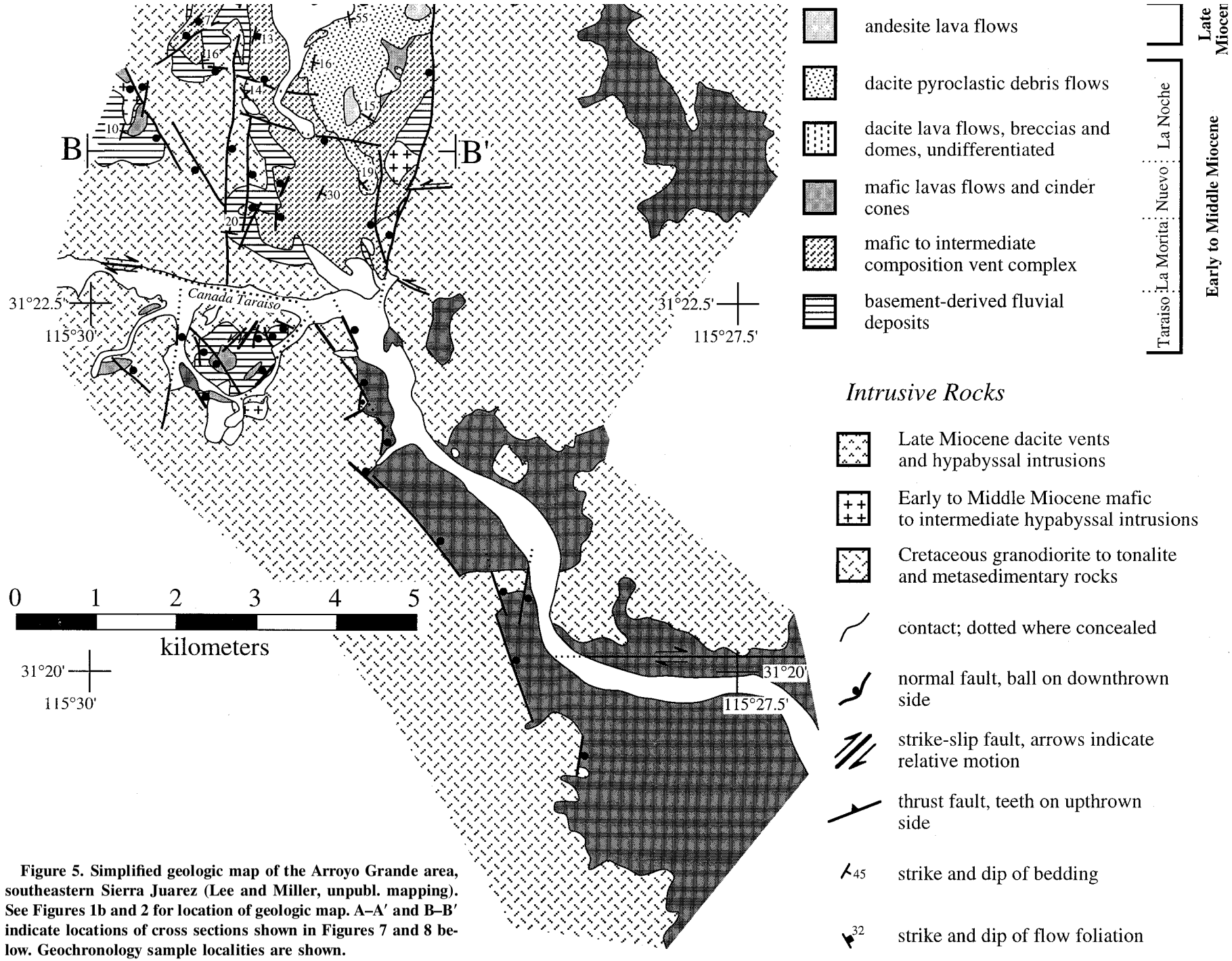

Figure 5. Simplified geologic map of the Arroyo Grande area, southeastern Sierra Juarez (Lee and Miller, unpubl. mapping). See Figures 1b and 2 for location of geologic map. A–A′ and B–B′ indicate locations of cross sections shown in Figures 7 and 8 below. Geochronology sample localities are shown.

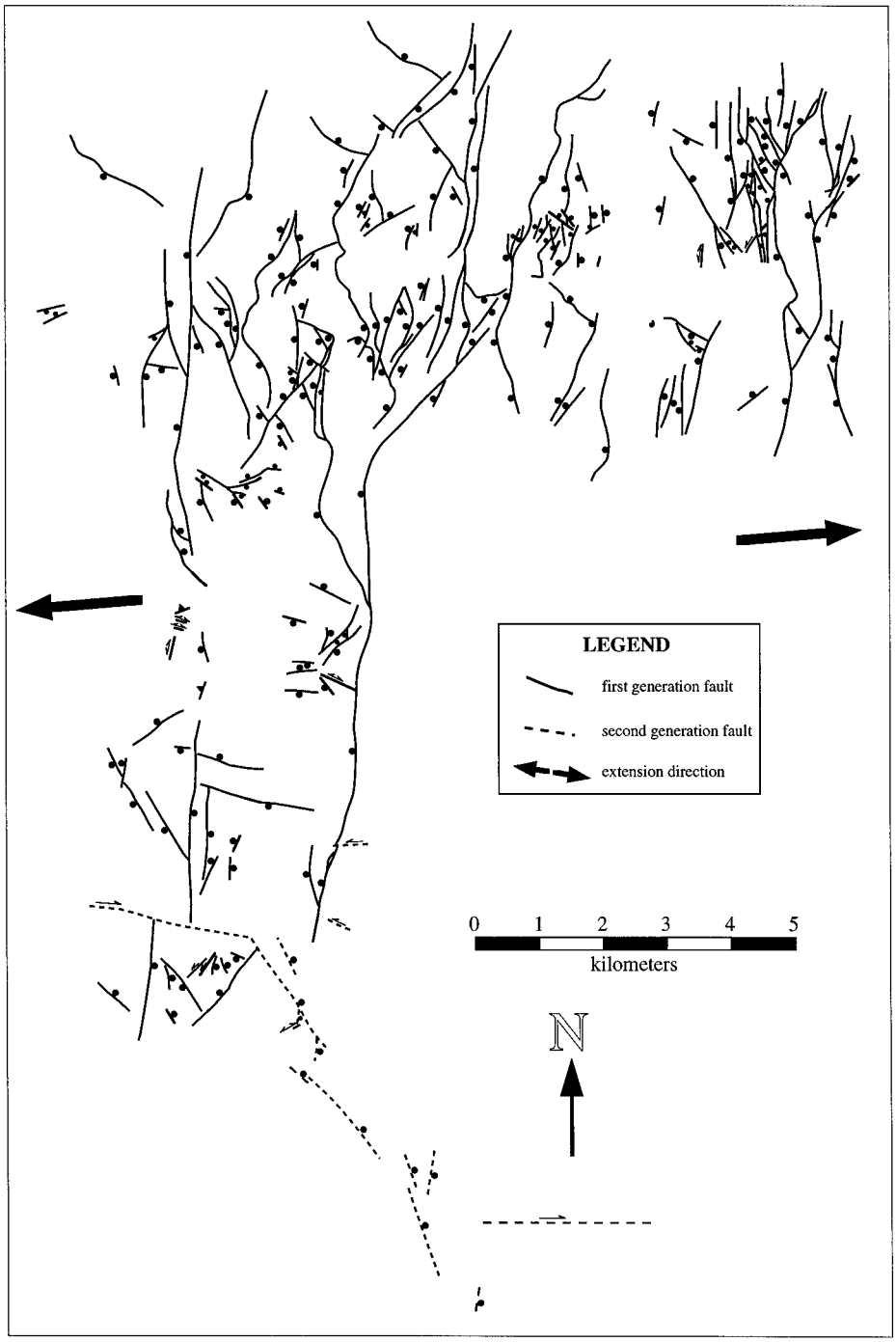

Figure 6. Fault map of the Arroyo Grande area showing the two generations of faults.

Emplacement of one intrusion deformed the Miocene volcanic section, which now dips ≈50° away from the intrusive contact. A $^{40}Ar/^{39}Ar$ hornblende age from this plutonic body is 10.96 ± 0.05 Ma (Figs. 3 and 4). Because this hypabyssal intrusion was emplaced at shallow levels (≤1 km), we interpret this age as a crystallization age, thereby providing a lower age limit on the timing of normal faulting.

Pliocene–Quaternary Units. Lower–middle Miocene volcanic and sedimentary rocks are locally unconformably overlain by nearly flat-lying Pliocene–Quaternary conglomerate, sand, scarce biotite-bearing tuff, and colluvium (Fig. 5). Conglomerate deposits consist of massive heterolithologic, subangular to rounded, pebble- to boulder-sized (as much as and more than 1 m across) granitic, basaltic, dacitic, and metasedimentary clasts. Sand deposits are dominated by well-bedded and cross-bedded, coarse-grained quartzofeldspathic sand with lesser basalt sand. These are fluvial and flash flood deposits and are informally referred to as proto–Arroyo Grande deposits. These deposits are typically preserved as 2–5 m thick, nearly flat-lying, abandoned stream terraces, although locally, sections are tens of meters thick. At least three generations of stream terraces are exposed at 110–120, 90–100, and 20 m above the present-day steam level.

Colluvium is locally extensive in the field area. Clasts range in size from pebbles to boulders. This locally derived, heterolithologic deposit is generally unconsolidated, but locally caliche cemented. The colluvium can be thick enough to obscure bedrock on gentle slopes. In places it covers the Quaternary fluvial deposits as well as the lower–middle Miocene volcanic and sedimentary rocks.

STRUCTURAL CHRONOLOGY

Introduction

On the basis of detailed mapping of 105 km^2 at 1:25 000 scale in the Arroyo Grande area, southern Sierra Juarez, we have identified two generations of faults: (1) a first generation comprised of primarily north-south–striking, east- and west-dipping normal faults; lesser, variably oriented strike-slip faults; and few east-west–striking, north- and south-dipping normal faults; and (2) a second generation of east-west–striking strike-slip faults and northwest-striking, northeast-dipping normal faults (Figs. 5 and 6). Reconnaissance mapping and interpretation of aerial photographs and remote sensing imagery suggest that first-generation faults likely extend over an area of at least 370 km^2. Locally, more small offset (<0.5 m) first-generation faults exist than could be incorporated onto our 1:25 000-scale field maps; where appropriate, the cumulative offset along these faults was incorporated onto nearby larger offset faults. In addition, large areas of Quaternary colluvium prevented mapping of all individual faults.

First-Generation Faults

First generation faults consists of three sets: (1) a dominant set of northwest- to northeast-striking, steeply west-dipping normal faults; (2) a subordinate set of northwest- to northeast-striking, steeply east-dipping normal faults; and (3) a lesser set of

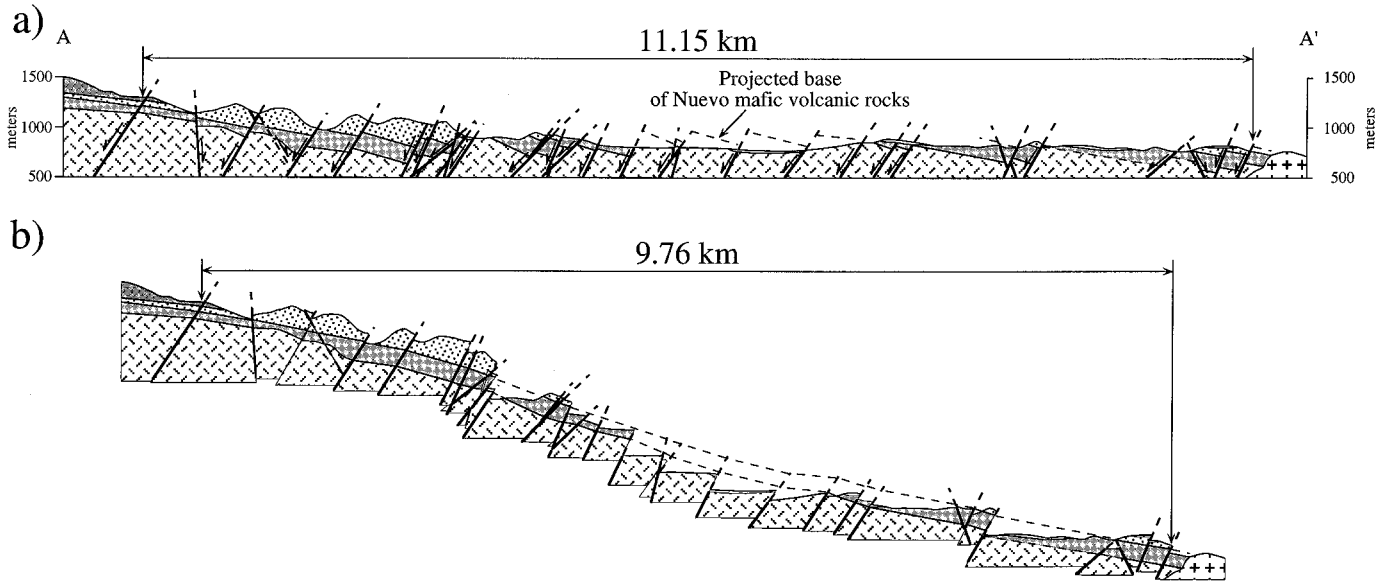

Figure 7. (a) Interpretative east-west cross section A–A′ across the northern part of the map area. (b) Palinspastic restoration of cross section shown in (a). See Figure 5 for location of cross section.

northwest- to northeast-striking, moderate to steeply east- and west-dipping strike-slip faults (Figs. 5 and 6). All three fault sets cut basement rocks and the Miocene sedimentary and volcanic succession. In addition, all three fault sets occur in a continuum; they have similar orientation and are distinguished solely on the basis of fault striation rake (faults with rakes of ≥45° were assigned to the normal fault population; faults with rakes of <45° were assigned to the strike-slip fault population). A few east-west–striking, north- and south-dipping normal faults and two north-northeast–striking, northwest-dipping thrust faults that also cut basement rocks and the Miocene sedimentary and volcanic succession have been mapped (Figs. 5 and 6). However, because these faults are few in number and poorly exposed, their kinematics and tectonic significance are not known.

The southern part of the map area is characterized by a relatively narrow zone of faulting with a few relatively widely spaced west- and east-dipping normal faults (Figs. 5 and 6). The predominant fault type in this area is a north-south– to north-northeast–striking, steeply west-dipping normal fault with a dip-slip displacement of ≈270 m (Figs. 5, 6, and 8). To the north, this single normal fault appears to splay into a series of generally northwest- to northeast-striking, steeply west-dipping normal faults that define a wider zone of deformation (Figs. 5, 6, and 7) Fault planes are commonly well exposed, especially within the La Noche dacite, with dips ranging from 90° to 31°; the average dip is ≈58° west (Fig. 9a). Slip along these faults varies from <5 m to as much as ≈200 m. In general, fault slip magnitude is inversely proportional to fault density. In the southern part of the map area, fault density is 1.0–1.6 faults/km, and fault slip is typically >50 m. In contrast, in the northern part of the map area, fault density is 2.0–3.0 faults/km, and fault slip is typically ≤20 m.

The dominant set of northwest- to northeast-striking, steeply west-dipping normal faults are antithetic to and strike obliquely to the north to north-northwest–striking down-to-the-east Main Gulf Escarpment, the Sierra Juarez range front fault exposed to the north and the Sierra San Pedro Martir range front exposed to the south. On the basis of our detailed mapping, the Main Gulf Escarpment is not present in the Arroyo Grande area.

The subordinate set of north-south– to northeast-striking, steeply east-dipping normal faults is primarily restricted to the northern part of the map area (Figs. 5 and 6). Well-exposed fault planes dip from 30° to 90°, averaging ≈58° east (Fig. 9b). Slip along these faults varies from <0.5 to 80 m. Consistent cross-cutting relationships were not observed between the west-dipping and east-dipping normal faults, suggesting that they moved concurrently.

Most of west- and east-dipping faults can be traced from as little as ≈0.5 km to several

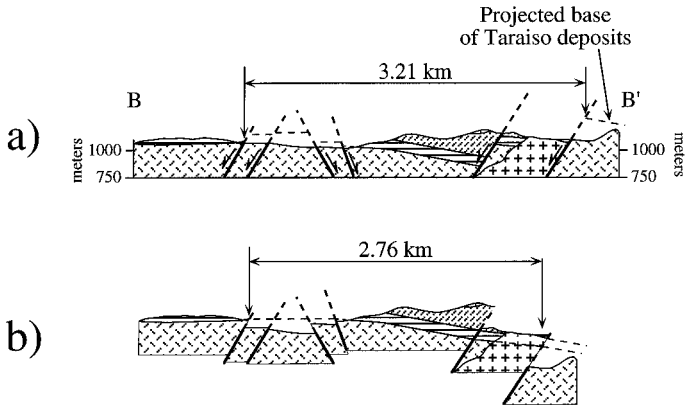

Figure 8. (a) Interpretative east-west cross section B–B′ across the southern part of the map area. (b) Palinspastic restoration of cross section shown in (a). See Figure 5 for location of cross section.

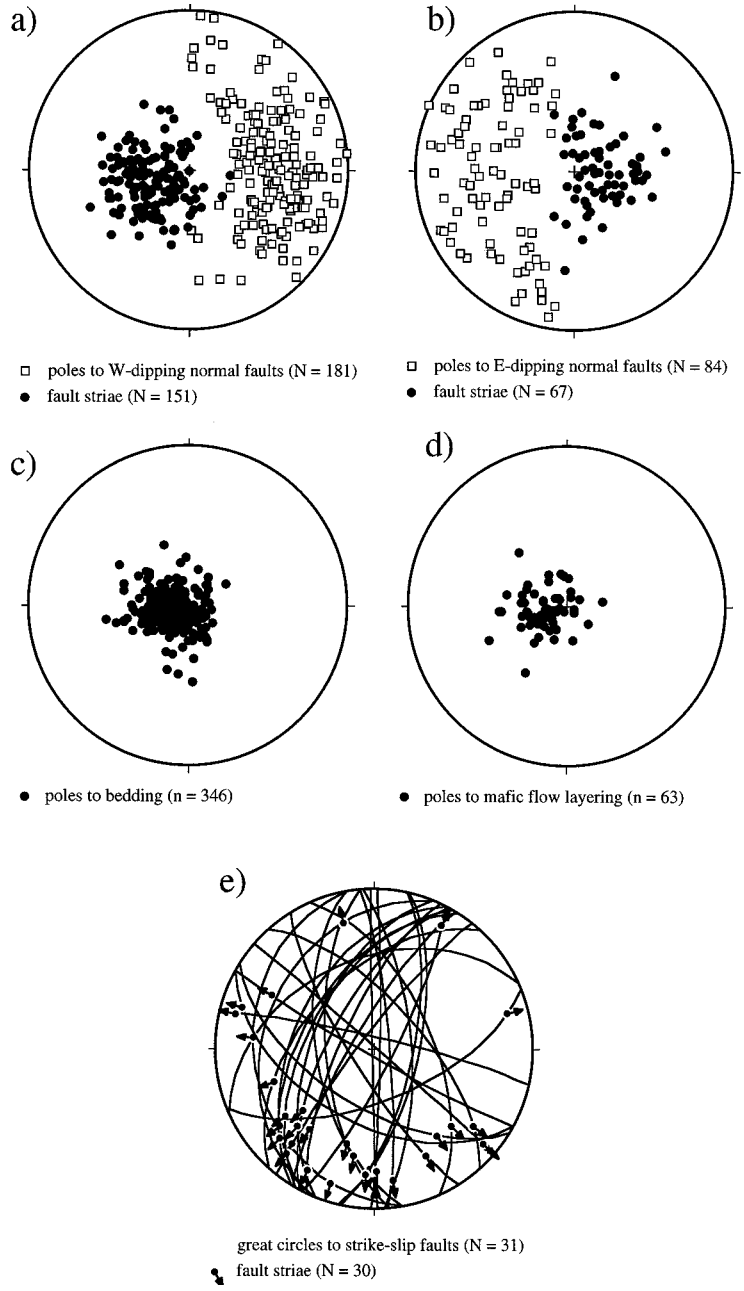

Figure 9. Structural data plotted on lower hemisphere, equal-area projections (number of measurements given in parentheses). (a) Poles to fault planes (open squares) and trend and plunge of fault striations (solid circles) for west-dipping normal faults. (b) Poles to fault planes (open squares) and trend and plunge of fault striations (solid circles) for east-dipping normal faults. (c) Poles to bedding from the Taraiso deposits and La Noche dacite. (d) Poles to mafic flow foliation from the Nuevo mafic volcanic rocks. (e) Great circles to strike-slip faults, trend and plunge of fault striations (solid circle) and slip direction (arrow).

kilometers. Faults are planar down-dip, but generally not so along strike (Figs. 5, 6, 7, and 8). Fault gouge and breccia are well developed, especially in the La Noche dacite, varying from centimeters to several meters in width. Both sets of normal faults also contain well-developed fault striations, which are defined by grooves, hydrothermal mineral lineations, calcite lineations, and small mullions; rakes vary from 90° to 46°. Similar faults with shallower fault striae are discussed as strike-slip faults below. On average, fault striations on the west-dipping faults indicate a slightly oblique slip direction (left-lateral; trend and plunge of 252, 63), and on the east-dipping faults a nearly pure dip-slip direction (trend and plunge of 90, 70; Figs. 9a and 9b). There is no correlation between fault dip and the rake of the fault striation (Fig. 10), with most of the faults exhibiting oblique slip.

The dominant west-dipping faults appear to control the dip of sedimentary and volcanic units within intervening fault blocks. Stratigraphic units within fault blocks dip uniformly ≈14° east; locally, dip magnitude is as much as ≈53° (Figs. 9c and 9d). The average bedding-to-fault-plane angle is 72°. The absence of noticeable deformation within the fault blocks (e.g., footwall uplift and hanging wall collapse) suggests that they behaved as rigid blocks during faulting.

A third set of poorly exposed minor, northeast- to northwest-striking, moderate to steeply east- and west-dipping strike-slip faults appears to be spatially and temporally associated with the more dominant normal faults (Fig. 9e). In most cases, the relative offset of these faults is unknown; in places, markers offset as much as 3–5 m indicate either right-lateral or left-lateral offset. Fault striations are typically well developed and rake as shallowly as 7° and as steeply as 44°, indicating a small oblique (normal) component of slip (Figs. 9e and 10). Most faults with steeper striae are discussed as normal faults; however, several of the normal faults possess both strike-slip and dip-slip striations. No consistent relative age patterns emerge from the scarce localities where the two sets of striations coexist. These relationships suggest that a small component of strike-slip motion accompanied or alternated with the dominant normal component.

West of the field area, first generation faults die out, and horizontal Miocene and younger strata overlie the Peninsular Ranges batholith on the more stable high plateau of the Sierra Juarez. Reconnaissance mapping and interpretation of aerial photography and Landsat TM images indicate that the dominant pattern of steeply west-dipping normal faults and east-dipping strata continues to the east-northeast of the field area.

The first generation faults offset the youngest dated La Noche dacite, which erupted at 15.98 ± 0.13 Ma. Deformation is older than the hypabyssal dacite dike that

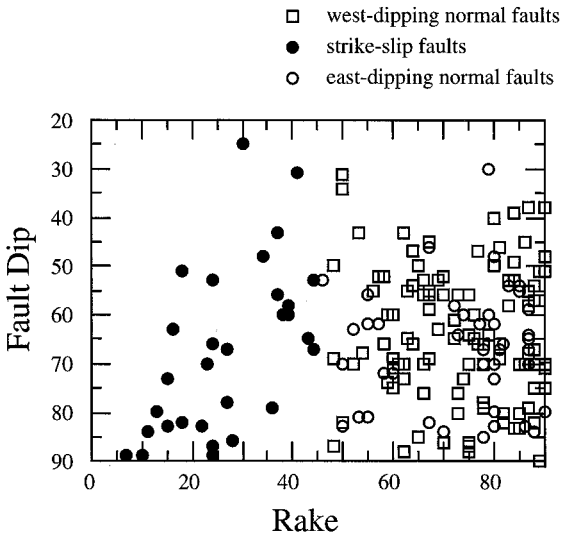

Figure 10. Plot of fault plane dip versus fault striation rake.

intruded a major west-dipping normal fault (see sample AG42; Fig. 5) at 10.96 ± 0.05 Ma. Thus the main phase of faulting occurred between 16 and 11 Ma and is middle–late Miocene in age.

Fault Kinematics. The geometry of faulting and the dip of layering, together with kinematic analysis of fault-slip data, constrain extension direction. First generation normal faults strike predominantly north-south and dip east or west, and bedding predominantly dips east, suggesting east-west extension (Fig. 9). Kinematic analysis of fault plane and striae orientations yields a more quantitative determination of extension direction (method of Marrett and Allmendinger, 1990). This method is a three-dimensional, incremental strain analysis that essentially converts each fault plane–striation pair into a fault plane solution. A linked Bingham distribution is then used to determine the principal axes of strain, thus providing an objective directional maximum for the extension and shortening axes. In essence this method determines an "average" orientation for the axes of a fault array. The calculated kinematic axes represent the orientations of the principal axes of strain: extension, shortening, and intermediate. Analysis of fault-slip data using this technique must meet the following criteria: (1) fault-slip data are scale invariant, (2) slip direction indicators have not been reoriented subsequent to faulting, (3) sampling is representative of the entire fault population, and (4) to some degree, the strain is spatially homogeneous (Marrett and Allmendinger, 1990).

In our study, fault-slip indicators from first generation faults appear to meet all four requirements. (1) Most first generation faults have offsets <50 m, although they show a range in offset of two orders of magnitude. Elsewhere, fault-slip data from faults with a range in offset of five orders of magnitude have been shown to be scale-invariant (Marrett and Allmendinger, 1990). (2) Reorientation of slip data appears unlikely because of the absence of postfaulting deformation in the area from which these data have been measured. (3) Excellent exposure allowed sampling representative of the entire fault population. (4) Finally, in the northern part of the area, where >95% of the data come from, strain appears to be spatially homogeneous.

Fault kinematic calculations for each population of first-generation faults yield nearly identical orientation for the extension axis: the extension axis is nearly horizontal east-west (azimuth of 265° and plunge of 6°; Fig. 11 and Table 2). This is not surprising for the east- and west-dipping normal faults, because field relationships indicate synchronous motion along the two fault populations. While the relative age relationships between strike-slip faults and normal faults are not straightforward, the kinematic analysis supports our field interpretation that minor strike-slip faulting accompanied normal faulting. As there is no evidence for younger folding or faulting that rotates the first generation faults, these results are inferred to record the original extension direction in present-day coordinates.

Magnitude of Extension. We estimated the magnitude of extension by palinspastically restoring the apparent down-dip displacement along faults within the upper 1 km of the crust across two cross sections, one in the northern part of the field area and one in the southern part of the area (Figs. 7 and 8). Because the fault blocks exhibit no evidence for internal deformation, we treat each as a rigid block. In the process of restoring these cross sections, no assumptions were made concerning whether these faults are planar or listric at depth, nor any regarding the geometry of underlying detachment faults. In the northern part of the field area, a palinspastic restoration of an east-west cross section, perpendicular to the general north-south strike of the normal faults, yields an estimate of ≈14% extension, assuming pure dip-slip motion along the normal faults (Fig. 7b). This restoration reveals a pre- to syn-faulting broad anticline in the Miocene strata. In the southern part of the area, a palinspastic reconstruction of the ap-

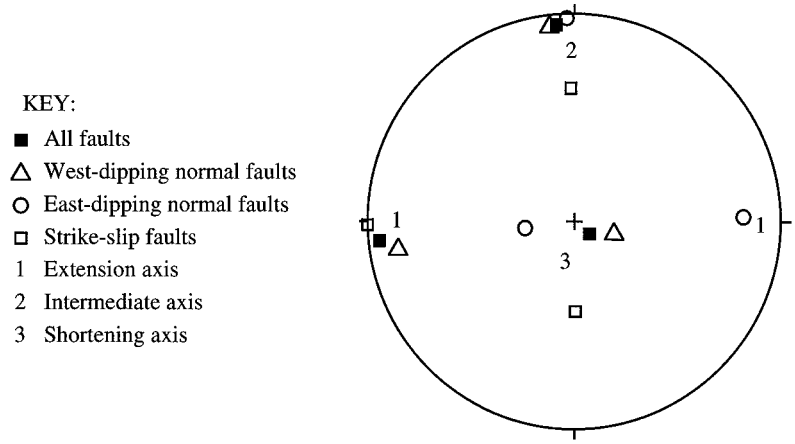

Figure 11. Stereonet plot of kinematic axes calculated for each set of first generation faults.

TABLE 2. RESULTS OF KINEMATIC ANALYSIS OF FIRST GENERATION FAULTS

Faults	Measurements	Trend and plunge*		
	(no.)	Shortening axis	Intermediate axis	Extension axis
All	275	126, 82	356, 5	265, 6
West-dipping normal	151	101, 74	354, 5	263, 15
East-dipping normal	68	257, 71	354, 2	85, 19
Strike-slip	56	174, 53	003, 37	270, 4

*All measurements in degrees.

parent offset along faults from an east-west cross section, parallel to the direction of extension, indicates ≈16% extension (Fig. 8b). This restoration also reveals a pre- to syn-faulting broad fold, although not nearly as well developed as to the north. These estimates are minima because (1) we are assuming pure dip-slip motion, not oblique-slip as indicated by the rake of fault striae, (2) of small offset (<0.5 m) faults that may not have been incorporated onto our maps, and (3) of faults that may be covered by Quaternary colluvium and were not included in our cross sections. Although the errors associated with these are difficult to quantify, especially for the last point, we believe that the magnitude of extension is probably no more than ≈18%.

Second-Generation Faults

Exposed in the southern part of the field area are second-generation faults comprised of en echelon, east-west–striking, right-lateral strike-slip faults, which are parallel to and probably related to the Agua Blanca fault, and northwest-striking, northeast-dipping normal faults (Figs. 5 and 6). One of the strike-slip faults is defined by the linear trace of Canada Taraiso and is locally exposed in an ≈1-m-wide fault zone defined by strongly fractured and crushed granite, and fault gouge and breccia. An exposed fault plane within this zone has an orientation of N61°W, 85°SW; associated fault striations indicate a slip direction of N64°W, 3°NW. This fault offsets a north-south–striking, east-dipping first-generation normal fault in the southern part of the field area by ≈570 m (Figs. 5 and 6). Thus this youngest fault postdates formation of the first-generation faults that are bracketed between 15.98 ± 0.13 and 10.96 ± 0.05 Ma. The second of these faults is also east-west–striking and is defined by an ≈7-m-high, linear escarpment in Quaternary older alluvium (Figs. 5 and 6), although no fault plane is exposed along this escarpment. On the basis of its similar orientation to the fault described above, as well as the Agua Blanca fault, we infer that it is a right lateral, strike-slip fault.

Associated with these strike-slip faults are a series of northwest-striking, northeast-dipping normal faults that cut Quaternary alluvial fan deposits and/or juxtapose hanging wall Quaternary alluvial fan deposits against footwall Cretaceous granitic rocks (Figs. 5 and 6). These faults are defined by a number of distinct geomorphic and structural relationships, including triangular facets, wineglass structures, and vertically offset drainages in the footwall; a sharp, linear break in topography at the granitic/alluvial fan contact; locally, an ≈7-m-high escarpment in the Quaternary alluvial fan deposits; and zones of fault gouge, cataclasis, and fracturing in granitic rocks at the fault contact. The preservation of these geomorphic features attests to the relatively young age of these faults. Because these normal faults and the strike-slip faults do not appear to cut and offset each other, we infer that they moved simultaneously.

Finally, the presence of at least three generations of abandoned Quaternary stream terrace deposits above the present-day stream level suggests uplift resulting from Quaternary normal faulting. Alternative interpretations for these older terraces include sea level change (e.g., Ortlieb, 1987) or stream capture by a drainage system with a lower base level, both of which are unlikely because the current drainage ends in a closed depression.

DISCUSSION

Middle–Late Miocene Structural Evolution

We have documented the oldest period of late Cenozoic extension in Baja California, thus our studies provide insight into the early structural evolution of the Gulf Extensional Province. First generation faults in the Arroyo Grande area are bracketed in age between 15.98 ± 0.13 and 10.96 ± 0.05 Ma. These faults are dominated by down-to-the-west normal faults, which are antithetic to the east-dipping Main Gulf Escarpment, and yet they are areally restricted to the western edge of the Gulf Extensional Province, which elsewhere is bounded by the Main Gulf Escarpment. Our mapping shows that the steeply east-dipping Main Gulf Escarpment does not cut through the Arroyo Grande area, although it is well exposed to the south along the Sierra San Pedro Martir range front and to the north along the central Sierra Juarez range front. These relations suggest simultaneous movement along the Main Gulf Escarpment and west-dipping faults in the Arroyo Grande area. Thus the Arroyo Grande area may delineate a broad zone whereby Main Gulf Escarpment slip is accommodated by smaller-magnitude slip along a series of antithetic normal faults. Initiation of movement along the Main Gulf Escarpment, however, is only well dated in southern Valle Chico at between 11 and 6 Ma (Stock and Hodges, 1990). If the younger age of the Main Gulf Escarpment from Valle Chico holds for areas adjacent to the Arroyo Grande area, then movement along the west-dipping faults may have initiated and ceased prior to the onset of movement along the Main Gulf Escarpment. In this context, movement along the Main Gulf Escarpment may have been accommodated in the Arroyo Grande area by broad folding (see Figs. 7b and 8b).

The west-dipping fault domain within the Arroyo Grande area is located in a region where the character of the Main Gulf Escarpment changes from south to north. To the south, the Sierra San Pedro Martir range front is a large-displacement (>5 km), down-to-the-east fault (Gastil et al., 1975). The pattern of west dips of Tertiary strata to the east suggests that this fault has a listric geometry defining an east-dipping detachment fault at depth (Dokka and Merriam, 1982; Stock and Hodges, 1990). In contrast, to the north, the Sierra Juarez range front appears to consist of both east- and west-dipping normal faults of small to moderate displacement (<100–500 m), which cut Miocene and younger strata that roll over to east dips across the escarpment zone (Axen, 1995). Axen suggests that this faulted, rollover anticline lies in the hanging wall of west-dipping detachment faults that lie to the east–east-northeast (Isaac, 1987; Siem and Gastil, 1994) and roots beneath the Sierra Juarez (Fig. 12a).

Our own reconnaissance geologic mapping and interpretation of aerial photography and Landsat TM images immediately north of the Arroyo Grande area suggest small to moderate displacement, east-dipping faults along the Sierra Juarez range front (Fig. 2). The dominant west-dipping normal faults of the Arroyo Grande area ap-

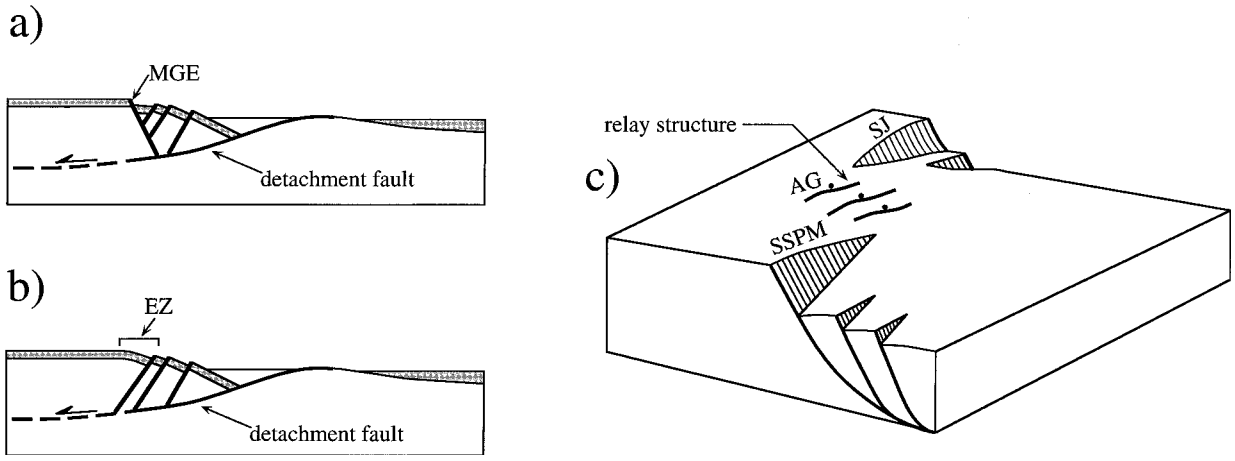

Figure 12. Highly schematic and generalized diagrams illustrating inferred geometries for the Main Gulf Escarpment zone. (a) Cross section across the northern Sierra Juarez showing geometry of Main Gulf Escarpment (MGE) and inferred underlying west-dipping detachment fault (modified after Axen, 1995). (b) Cross section across the Arroyo Grande area, southern Sierra Juarez showing geometry of roll-over anticline and west-dipping faults in the escarpment zone (EZ) above an inferred west-dipping detachment fault. (c) Alternative interpretation for the Arroyo Grande area. Three-dimensional diagram shows the Arroyo Grande area (AG) forming within a relay structure that connects the footwall of the Sierra San Pedro Martir range front fault (SSPM) with the hanging wall of the Sierra Juarez range front fault (SJ). See text for full discussion. Diagrams not to scale.

pear to gradually die out northward toward the central Sierra Juarez, and east-dipping normal faults, associated with the Main Gulf Escarpment, gradually die out southward from the central Sierra Juarez. We have not observed any major strike-slip or transfer faults between the two areas (Fig. 2). In addition, our studies in the Arroyo Grande area show that lower–middle Miocene strata are flat lying on the high plateau of the Sierra Juarez and dip east across the escarpment zone defining a faulted anticline (see Figs. 7b and 8b). Furthermore, our reconnaissance studies to the east-northeast of the study area indicate that the pattern of east-dipping strata cut by west-dipping normal faults continues, which suggests that an east-dipping detachment fault does not lie beneath this part of the Sierra Juarez. As with Axen (1995), we suggest that one possible interpretation of the observed faulted, roll-over anticline in the Arroyo Grande area is that it lies in the hanging wall of a west-dipping detachment fault, although such a fault has not yet been described from the little-studied area to the east (Fig. 12b). However, in the Arroyo Grande area there is no range front escarpment; rather, Miocene strata roll over from flat lying to east dips across the escarpment zone (cf. Figs. 12a and 12b).

If the Sierra San Pedro Martir range front fault shallows into an east-dipping detachment fault and a west-dipping detachment fault roots beneath the Sierra Juarez, then the southern part of our study area lies within a region of dip reversal in the underlying regional detachment fault systems. In extensional tectonic settings, such regions are accommodation zones (e.g., Faulds et al., 1990) or intervening transfer zones (e.g., Gibbs, 1984), which are oriented roughly parallel to the extension direction. Such zones accommodate structural and/or temporal changes that are orthogonal or oblique to the extension direction, such as dip reversals of the underlying detachment fault systems, areas of opposing tilt-block domains, and different extensional strain rates and/or different magnitudes of extension. Accommodation zones may be characterized by a single fault or a set of strike-slip or transfer faults (e.g., Gibbs, 1984; Lister et al., 1986), intermeshing conjugate normal faults (e.g., Faulds et al., 1990), or relay structures connecting footwall and hanging wall blocks of two en echelon faults (e.g. Larsen, 1988). The Agua Blanca fault, located south of the Arroyo Grande area, is a major east-west– to west-northwest–striking, right-lateral strike-slip fault that would provide an ideal transfer fault between the Arroyo Grande area to the north and the Sierra San Pedro Martir range front fault to the south (Fig. 2). However, the magnitude of extension decreases and dies out northward along the Sierra San Pedro Martir and southward from the Arroyo Grande area toward the Agua Blanca fault. Furthermore, the Agua Blanca fault appears to terminate just west of the northward projection of the Sierra San Pedro Martir range front fault (Allen et al., 1960; Rogers, 1970; Fig. 2). These field relationships suggest that there is little or no extension at the eastern termination of the Agua Blanca fault. Hence, the Agua Blanca fault does not appear to be an accommodation structure between dip reversals of the underlying detachment faults.

The en echelon geometry of the Sierra San Pedro Martir and Sierra Juarez range front faults (Fig. 2) may provide an alternative mechanism for the origin of the west-dipping fault domain in the Arroyo Grande area. In this en echelon geometry, the Arroyo Grande area lies along a relay structure (e.g., Larsen, 1988) that connects the footwall of the Sierra San Pedro Martir range front fault with the hanging wall of the Sierra Juarez range front fault (Fig. 12c). In this configuration, the antithetic west-dipping faults act as displacement transfer structures between the Sierra San Pedro Martir and Sierra Juarez range front faults. In this interpretation, the relay structure (i.e., the Arroyo Grande area) may overlie the dip reversal of the underlying detachment faults or the east-dipping detachment fault of the Sierra San Pedro Martir fault. If the latter is the case, then there must be an accommodation zone to the north of the Arroyo Grande area between east-dipping and west-dipping detachment faults.

Because of the lack of sufficient data on the deeper structure beneath the Arroyo

TABLE 3. EVIDENCE FOR EXTENSION, GULF EXTENSIONAL PROVINCE, MEXICO

Key*	Area (age of extension)	Summary of evidence	References
Western Gulf extensional province—Baja California			
1	Sierra Las Tinajas (unknown)	Geologic mapping and aerial photographic interpretation in the northern part of the range indicate that the volcanic sequence is flat lying, whereas the remainder of the range is characterized by northwest-striking, west-tilted blocks cut by east-dipping, northwest-striking normal faults (a).	(a) Gastil et al., 1975
1	Sierra Las Pintas (post–late Miocene)	In the northern part of the range, north-northwest– to northeast–striking faults postdate 7.6 ± 0.4 Ma basalt (a), and in the southern part, northeast-striking faults cut 8.9 ± 0.6 Ma and 9.5 ± 1.0 Ma andesite and dacite, respectively (b), indicating post–late Miocene extension.	(a) McEldowney, 1970; (b) James, 1973
2	Southern Sierra Juarez (middle Miocene)	Kinematic analysis of fault-slip data indicates east-west extension along primarily north-south–striking, steeply west-dipping normal faults. Timing of extension is bracketed between 15.98 ± 0.13 and 10.96 ± 0.05 Ma. Magnitude of extension is 14%–16% (a).	(a) This paper
3	Sierra Santa Rosa basin (late Miocene–early Pliocene)	North-northeast–striking normal faults dip 20°E. Westward tilted middle Miocene volcanic rocks in the hanging wall are overlain by Pliocene fanglomerates in angular unconformity, providing evidence for late Miocene–early Pliocene extension. Fault striations indicate that the direction of extension is approximately to the southeast (a).	(a) Bryant, 1986
4	Sierra San Pedro Martir (late Miocene–Holocene)	Along the southern part of the north-northwest–striking Sierra San Pedro Martir Range front fault, 11 Ma and older volcanic rocks do not show a variation in thickness. Hence, the escarpment fault was not active until post–11 Ma (a). Paleoseismic studies of stream terraces along Holocene fault scarps along the same range front fault, but farther to the north, indicate periodic fault motions ranging in age from at least 3520 ± 90 to 130 ± 40 yr B.P. (b, c).	(a) Stock and Hodges, 1990; (b) Gastil et al., 1975; (c) Brown, 1978
4	Southern Valle Chico (late Miocene)	Extension occurred along north– to north-northwest–striking, high-angle east- and west-dipping normal faults. Extension initiated between eruption of volcanic rocks that yield ages of 10.85 ± 0.16 and 6.1 ± 0.06 Ma (a). The magnitude of extension is estimated to be 10%, of which half occurred prior to 6 Ma and the other half since 6 Ma (a).	(a) Stock and Hodges, 1990
4	Puertecitos region (late Miocene and younger)	Here, steeply dipping 7.3 ± 1.5 to 8.3 ± 0.8 Ma volcanic rocks are overlain by flat-lying 5.9 ± 0.2 Ma rhyolites (a, b), indicating a late Miocene age for faulting. Numerous north– to north-northwest–striking, east-dipping synthetic and west-dipping antithetic normal faults cut the post–6 Ma volcanic rocks (a, c), indicating extension continued into post-Miocene time.	(a) Gastil et al., 1975; (b) Gastil et al., 1979; (c) Dokka and Merriam, 1982
5	Sierra San Fermin (late Miocene–Pliocene/Quaternary)	A sequence of late Miocene rhyolite ignimbrites are cut by normal faults indicating onset of extension between 11.0 and 6.0 Ma. Inversion of fault-slip data indicates an east-west to east-northeast–west-southwest direction of extension during late Miocene–Pliocene/Quaternary time. Reconstructions indicate 7%–24% extension (a).	(a) Lewis, 1994
6	Sierra Agua de Soda (Miocene(?)–Pliocene)	Along the southern flank of the range, normal faults cut and tilt Miocene(?) volcanic rocks, which are unconformably overlain by flat-lying Pliocene fluvial and marine deposits (a, b). The volcanic rocks are tilted moderately to the east and west by north-south– to west-northwest–east-southeast–striking, steeply west- and east-dipping normal faults (a). The faults exhibit vertical offsets that vary from a few meters to tens of meters (a). Kinematic analysis of fault-slip data indicates extension in a east-northeast to west-southwest direction with nearly dip-slip motion (a). Magnitude of extension is estimated at 17% (a).	(a) J. Lee , unpub. mapping; (b) Gastil et al., 1975
7	Sierra Los Paredones (late Miocene)	At the northern end of the range, normal faults cut and tilt 12.7 ± 0.5 Ma to 10.5 ± 0.4 Ma volcanic rocks, which are unconformably overlain by ca. 5 Ma basalts (a, b), suggesting late Miocene faulting. In the central part of the range, normal faults strike northwest-southeast and dip steeply to the northeast and southwest; bedding strikes roughly north-south and dips shallowly to moderately to the west. Kinematic analysis of fault-slip data indicates extension in an east-northeast–west-southwest direction (a). Magnitude of extension is estimated at 5% (a).	(a) J. Lee, unpub. mapping; (b) Gastil et al., 1975
8	Santa Rosalia area (late Miocene–Holocene)	Here, 19.9 ± 0.6 Ma to 10.7 ± 0.3 Ma andesites, tilted up to 45° along north– to north-northwest–striking, west-dipping normal faults (a, b), are overlain unconformably by lower Pliocene (c) or uppermost Miocene rocks (b). Immediately to the north, movement on the Main Gulf Escarpment and associated north-northwest–striking normal faults cuts a 10 Ma basalt (b). The associated north-northwest–striking normal faults are overlain by 3 Ma basalts, and yet some faults appear to be coeval with the eruption of Pliocene–Holocene alkalic volcanic rocks in north-northwest–trending grabens (b). These relations indicate that extension was either continuous or episodic from late Miocene to Holocene time. Paleostress analyses from fault plane and striae orientations show that late Miocene north– to north-northwest–striking, east- and west-dipping normal faults formed in response to northeast-southwest–oriented least horizontal stress (σ_3) and that motion on faults with the same orientation during the Pliocene was oblique with σ_3 oriented west-northwest–east-southeast to east-west (d).	(a) Wilson and Veytia, 1949; (b) Sawlan and Smith, 1984; (c) Wilson and Rocha, 1955; (d) Angelier et al., 1981

Grande area, the interpretations presented above are no more than reasonable inferences of the three-dimensional geometry in the region. Clearly, further work, especially seismic reflection data, is needed in order to document the geometry of the underlying detachment fault system in the Arroyo Grande and adjacent areas, and thereby fully characterize the development of this accommodation zone.

Late Cenozoic Extension in the Gulf Extensional Province

This study of the geometry, kinematics, magnitude, and timing of normal faulting in the southern Sierra Juarez is part of a growing body of evidence for extensional deformation throughout the Gulf Extensional Province of Baja California and northwestern mainland Mexico that has been steadily accumulating during the past 25–30 yr (Table 3). In general, east-west extension within the Gulf Extensional Province has persisted from middle Miocene to present day, although movement along normal faults has not been synchronous throughout the province. In the western Gulf Extensional Province, along Baja California, structural patterns show northwest- to northeast-striking normal faults that generally dip steeply to moderately both west and east, and stratal tilts within fault blocks vary from shallow to moderate (see summary of evidence for sites 1–11 in Table 3 and Fig. 13). Ages of pre- and postfaulting volcanic rocks from a number of areas indicate that extension began primarily during late Miocene time. Our study provides the oldest reported constraints on timing of extension in this part of the Gulf Extensional Province, where it is of middle–late Miocene age.

Faulting continues today as indicated by Holocene scarps along the southern part of the north-northwest–striking San Pedro Martir fault, and by some faults that appear

TABLE 3. *(Continued)*

Key*	Area (age of extension)	Summary of evidence	References
9	Bahia Concepcion area (post–late Miocene, pre–late Pliocene)	Reconnaissance mapping shows that 9.8 ± 1.6 Ma and 8.0 ± 3.7 Ma volcanic rocks (a) are tilted to the northeast up to 45° by northwest- and northeast-striking normal faults (b). Overlying these rocks, in angular unconformity, are Pliocene marine rocks indicating pre–late Pliocene normal faulting.	(a) Gastil et al., 1979; (b) McFall, 1968
10	Loreto Basin (late Pliocene)	Northwest– to north-northwest–striking, shallow to steeply west-dipping normal faults (a) are active throughout basin sedimentation, from ca. 3.4 Ma to 2.36 Ma (b). A few faults cut deposits younger than 2.36 Ma, suggesting that most of the faulting is late Pliocene in age (b). Kinematic analysis of fault-slip data indicates extension in an east-west to east-southeast–west-northwest direction. Magnitude of extension is estimated at between 35% and 58% (a).	(a) Stone, et al., 1994; (b) Umhoefer, et al., 1994
10	Loreto area (post–middle Miocene–Present)	Reconnaissance mapping shows that early Oligocene–middle Miocene rocks locally dip more steeply than 10°–30°–dipping Pliocene rocks, indicating pre-Pliocene faulting. Quaternary alluvial rocks are locally cut by north-northwest–striking normal faults, indicating that normal faulting continues to present time (a).	(a) McLean, 1988
11	La Paz area (post–middle Miocene)	Northwest-striking, east-dipping normal faults offset 12.5 ± 1.4 Ma volcanic rocks (a), providing evidence for post–middle Miocene extension. Locally, however, the area is characterized by flat-lying Miocene units.	(a) Hausback, 1984
Eastern Gulf extensional province—Isla Tiburon and mainland Mexico			
12	Isla Tiburon (middle–late Miocene)	Normal faults have a variety of orientations, although northwest- and northeast-striking faults appear to be the dominant sets (a). Here, 19–15 Ma volcanic rocks dip up to 50°, whereas 13–11 Ma volcanic rocks dip only 25°, indicating onset of normal faulting between 15 and 13 Ma. Flat-lying 6–4 Ma rocks provide evidence that faulting had ceased by that time (b).	(a) Gastil et al., 1974; (b) Neuhaus et al., 1988
13	Coastal Sonora region (late Miocene)	Volcanic rocks >10–12 Ma dip up to 60° to the east along northwest-striking normal faults, and 7.0 ± 0.3 Ma volcanic rocks are flat lying, providing evidence for late Miocene extension (a).	(a) Gastil and Kummenacher, 1977
14	Southern Sonora and southern Chihuahua (unknown)	North-northwest–striking, east- and west-dipping normal faults cut Tertiary volcanic rocks of unknown absolute age (a).	(a) King, 1939
15	Northern Sinaloa (unknown)	North-northwest–striking, northeast-dipping normal faults cut Tertiary volcanic rocks of unknown absolute age (a).	(a) Fredrikson, 1971
16	Southern Sinaloa (between middle Miocene and Quaternary)	Here, strata dip in general 20°–40°, but as much as 65°, to the west along north-northwest–striking, near-vertical to 22° east-dipping normal faults. Secondary east-northeast–striking normal faults are present (a, b). Normal faults offset volcanic rocks as young as 16.8 ± 0.3 Ma, and Quaternary basalts are flat lying, providing evidence for middle Miocene–Quaternary extension. Fault geometry and paleostress analysis of fault-slip data suggest that the least horizontal stress (s_3) direction was east-northeast. Magnitude of extension is estimated at 20%–50% (b).	(a) Henry and Fredrikson, 1987; (b) Henry, 1989
17	West-central Nayarit (middle–late Miocene)	Here, 21.1 ± 0.2 to 13.8 ± 3.0 Ma volcanic and associated sedimentary rocks dip 20°–30° to the northeast along northwest-striking normal faults (a). Basalts, and locally rhyolites, dated at 10–8 Ma (b) lie in angular unconformity above this older sequence, but are themselves cut by the normal faults. Normal faults are overlain by Pliocene–Holocene volcanic rocks, providing evidence for middle–late Miocene extension.	(a) Gastil et al., 1978; (b) Gastil et al., 1979
18	Bahia de Banderas area (post–late Miocene)	Here, 11 Ma tuffs and 10 Ma basalts are tilted up to 36° along north-south–striking normal faults, indicating east-west extension in post–late Miocene time.	(a) Jensky, 1974

*See Figure 13 for locations of areas discussed.

to be coeval with the eruption of Holocene alkalic volcanic rocks in north-northwest–trending grabens in the Santa Rosalia area (sites 4 and 8; Table 3 and Fig. 13). Estimates of extension direction from regional fault and tilt patterns, paleostress analysis, and kinematic analysis indicate extension in an east-west to northeast-southwest orientation. Estimates of the magnitude of extension range from 2% to 58%.

The eastern Gulf Extensional Province, including Isla Tiburon and mainland Mexico, shows a similar style and timing of extension. The oldest age constraints on normal faulting within the eastern Gulf Extensional Province are reported from Isla Tiburon (site 12; Table 3 and Fig. 13). There, 19–15 Ma volcanic rocks dip as much as 50°, whereas 13–11 Ma volcanic rocks dip only 25°, indicating that normal faulting was active between 15 and 13 Ma. Flat-lying, 6–4 Ma rocks mark the local cessation of normal faulting. Elsewhere in the eastern part of the Gulf Extensional Province, the onset of east-west–directed extension occurred during late Miocene time (sites 12–18; Table 3 and Fig. 13). The magnitude of extension is locally as much as 50%.

These structural and geochronologic data confirm a period of extension in Baja California that predated the onset of sea-floor spreading in the Gulf of California at 4–5 Ma (Moore and Buffington, 1968; Larson et al., 1968) as suggested by a variety of other geologic data, including middle–upper Miocene marine sedimentary rocks that are exposed at various localities along the length of the peninsula and on islands within the Gulf of California (McCloy and Ingle, 1982; Boehm, 1984; Ingle, 1973, 1974, 1984; McCloy, 1984; Smith et al., 1985; Smith, 1991), and seismic reflection profile data from within the gulf that suggest pelagic sedimentation prior to opening of the gulf (Moore and Buffington, 1968; Moore, 1973).

Origin of Proto-Gulf Extension

Geochronologic data on the timing of arc-related volcanism and timing and magnitude of extension in the southern Sierra Juarez agree nicely with the global plate reconstruction model of Stock and Hodges (1989) and are also consistent with the suggestions of Humphreys and Weldon (1991) and Engebretson et al. (1985). By 16 Ma, arc-related volcanism within the southern Sierra

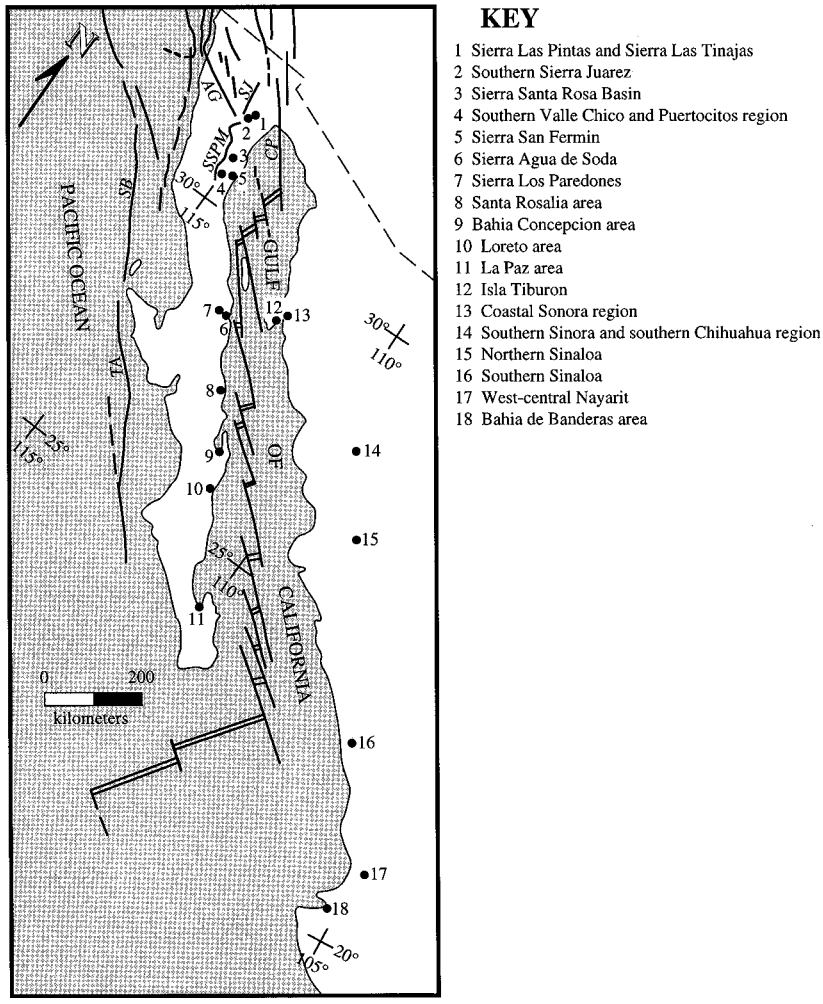

Figure 13. Map showing location of study areas within the Gulf Extensional Province that are discussed in the text and Table 3. Numbers are keyed to Table 3. Abbreviations for major faults: AG, Agua Blanca; CP, Cerro Prieto; SB, San Benito; SJ, Sierra Juarez; SSPM, Sierra San Pedro Martir; TA, Tosco-Abreojos.

Juarez had ceased. The global plate reconstruction model shows that at this time the Rivera triple junction had migrated southward of the latitude of the Sierra Juarez, and subduction had ceased and had been replaced by a growing right-lateral strike-slip boundary (Figs. 14a and 14b). Our study indicates that the main phase of normal faulting, an episode of east-west extension, is bracketed between 15.98 ± 0.13 and 10.96 ± 0.05 Ma, clearly postdating cessation of subduction and supporting a distinctly proto-gulf phase of extension (Fig. 14b). Global plate reconstructions indicate that, sometime between 15 and 9 Ma, relative plate motions between the Pacific and North American plates at this latitude changed from parallel to the margin to transtensional (Stock and Hodges, 1989), although a fixed hotspot reference frame model indicates transtensional plate motion may have begun as early as 17 Ma (Engebretson et al., 1985; Fig. 14c). The constraints on middle Miocene (16–11 Ma) extension reported in this study do not discriminate between these two models, but are broadly consistent with both. We suggest that the middle Miocene episode of east-west extension in the Arroyo Grande area was a direct response to the onset of transtensional, relative plate motion. Because no extension occurred along the western margin of Baja California at this time (Spencer and Normark, 1979; Hausback, 1984), the transtensional plate motion was partitioned into two components: a strike-slip component parallel to the San Benito and Tosco-Abreojos faults along the western margin of Baja California, and a nearly orthogonal extensional component within what is now the Gulf Extensional Province (Stock and Hodges, 1989; Fig. 14c).

Humphreys and Weldon (1991), however, have argued that dextral transform motion must have been ongoing by 17 Ma within the proto-gulf region, because Pacific–North American plate motion since 4–5 Ma could not have accounted for the minimum geologic separation of Baja California from mainland Mexico. If a strong dextral component of deformation characterized middle Miocene deformation, it was not manifested within the Arroyo Grande area. While the geologic separation across the gulf points to proto-gulf dextral faulting, such faulting is only known to have become active in the Gulf Extensional Province possibly during late Miocene time and certainly during Pliocene time (Lewis, 1994; also Table 3).

We can test the idea of a strong component of middle–late Miocene dextral motion by comparing it to small-scale analytical and experimental (soft clay and sand-silicone) modeling of oblique rifting (e.g., Withjack and Jamison, 1986; Tron and Brun, 1991). Such models describe the relationship between rift orientation and extension direction in order to characterize a possible transtensional component in the system. Withjack and Jamison (1986) define the following parameters: γ is the angle between rift strike and the extension direction; α, the acute angle between rift strike and relative displacement direction between opposite sides of the rift, is a measure of the degree of oblique rifting and is defined by $\cot \alpha = 2 \tan (90-\gamma)$. Smaller values of α therefore indicate a larger degree of oblique rifting. As with any empirical model, caution is needed when extrapolating to natural examples. In this case, drawbacks with the experimental systems are scale, time, and the use of homogeneous materials.

In our study area, the Main Gulf Escarpment is the best approximation of middle–late Miocene rift orientation and strikes ≈342° in northernmost Baja California. The extension direction for middle–late Miocene faulting in the Arroyo Grande region is 265°, and the average strike of normal faults is 355°–357°. These values yield $\gamma = 77°$ and $\alpha = 60°$. Therefore, the displacement direction between opposite sides of the rift is 282°, 17° clockwise from the extension direction. In addition, the analytical and clay models of Withjack and Jamison (1986), for the values cited here, predict that normal faults will develop ≈15° clockwise from the rift strike in excellent agreement with the

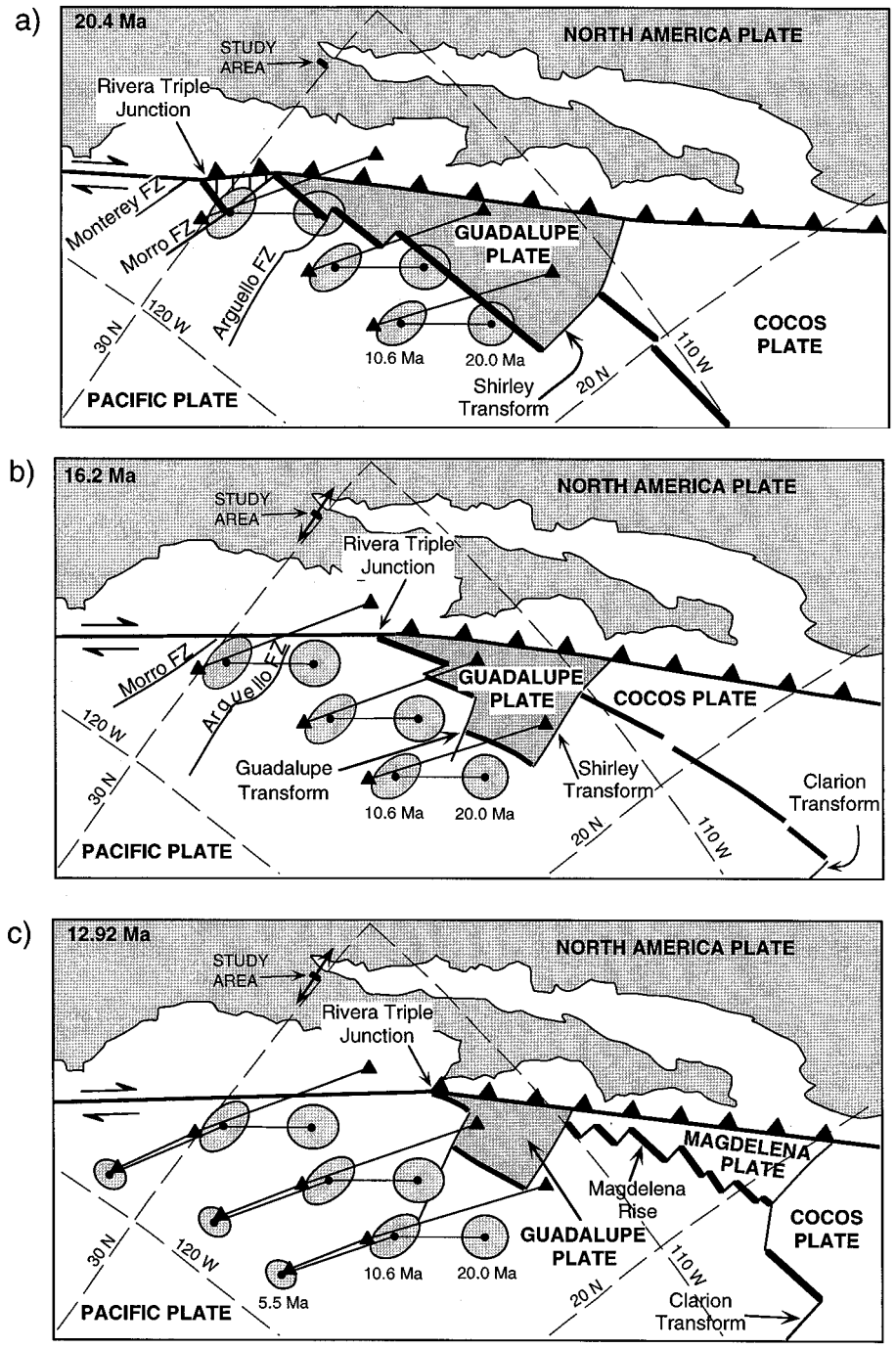

Figure 14. Plate configurations with respect to Baja California and the study area for time periods (a) 20.4 Ma, (b) 16.2 Ma, and (c) 12.9 Ma. Extension direction for the study area, bracketed between 15.98 ± 0.13 and 10.96 ± 0.05 Ma, is shown in (b) and (c) by the double-headed arrow. Reconstructions are based on global plate reconstructions of the Pacific plate to the North American plate of Stock and Molnar (1988). In addition, 130 km of east-northeast extension has been removed from the Basin and Range Province of Mexico (see Stock and Lee, 1994). Past positions of points and 95% confidence regions at 20.0, 10.6, and 5.5 Ma on the Pacific plate relative to fixed North America are from Stock and Hodges (1989). Solid triangles are positions of points at 17, 9, and 5 Ma based on the fixed hotspot reference frame of Engebretson et al. (1985). Maps are an oblique Mercator projection modified after Stock and Lee (1994).

angular relationship between the average strike of normal faults in the Arroyo Grande area and strike of the Main Gulf Escarpment. Therefore, comparison of normal fault development and extension in the Arroyo Grande area to analytical and clay models of oblique rifting indicate only a minor component of dextral motion during the middle–late Miocene, in general agreement with the paucity of strike-slip indicators in the Arroyo Grande area from that time interval. Hence, dextral motion was not an important component of the evolution of the Gulf Extensional Province until after middle–late Miocene time.

Post–Late Miocene Structural Evolution

If our inference of simultaneous movement along second-generation strike-slip and normal faults in the southern part of the field area is correct, then these faults define a right-step in a right-lateral strike-slip fault system. In this configuration, the northwest-striking, northeast-dipping normal faults act as displacement transfer structures between en echelon strike-slip faults. Such a geometry between strike-slip and normal faults has been well known since displacement transfer normal faults were first described by Burchfiel and Stewart (1966) and Crowell (1974). This geometry appears to provide a mechanism for accommodating transfer of slip from the Gulf Extensional Province to the Transpeninsular Strike-slip Province. Because of the well-preserved geomorphic features associated with these second-generation faults, fault slip is Quaternary, or possibly Pliocene, in age.

CONCLUSIONS

Volcanic and fluvial strata form a carapace on crystalline rocks of the Peninsular Ranges batholith in the southern Sierra Juarez. Most of the volcanic rocks are middle Miocene in age; fluvial deposits may be somewhat older. These deposits record development of a broad, stable, river-worked tableland, where mafic and intermediate magmatism was related to the waning stages of subduction, or outlasted the transition to a rift-transform margin.

The main deformational fabric comprises three sets of related faults: a dominant set of north-south–striking normal faults that are west-dipping, a secondary set of north-south–striking faults that are east-dipping, and lesser strike-slip faults. All three sets of faults have a common extension direction

(265°) and are temporally and spatially related. East-west extension occurred along these faults between 15.98 ± 0.13 Ma and 10.96 ± 0.05 Ma, attesting to deformation that is distinctly older than evolution of the oceanic rift. Deformation also may have preceded known initiation of the Main Gulf Escarpment between 11 and 6 Ma, which is only well dated in southern Valle Chico (Stock and Hodges, 1990). The primarily down-to-the-west normal faulting may have been a precursor or an early phase accommodation zone along the escarpment.

Faulting related to the modern kinematics of the Transpeninsular Strike-slip Province is also present, consisting of east-west–striking, right lateral strike-slip faults, and connecting northwest-striking, northeast-dipping normal faults. The strike-slip faults are parallel to and probably related to the nearby Agua Blanca fault; the normal faults are displacement transfer structures between en echelon strike-slip faults and probably provide a mechanism for transfer of slip from the Gulf Extensional Province to the Transpeninsular Strike-slip Province.

The timing of east-west extension documented in the southern Sierra Juarez coincides with the calculated onset of transtensional plate motions between North American and Pacific plates. This observation supports the hypothesis that middle Miocene transtensional plate slip was partitioned into two components: a strike-slip component parallel to active faults along the western margin of Baja California, and an extensional component, orthogonal to the margin but located in what is now the Gulf Extensional Province. Hence, the onset of extension within the circum-gulf region occurred in response to a change in the plate boundary configuration.

ACKNOWLEDGMENTS

This research was supported by grants from the National Aeronautics and Space Administration and the National Science Foundation (EAR-9305131). We thank the many people who assisted us in the field, including W. Bohrson, O. Castro, T. Dixon, E. Gamiz Ramirez, A. Grunder, G. Lopez Morteo, L. Mariano, A. Miner, C. Santin, and H. Trinedad Melendez (with Lee); and P. Gans, G. Gonzalez, R. Spelz, F. Zamora Arroya, and M. Rebolleda Vieyra (with Miller). A. Gutierrez is gratefully acknowledged for his hospitality and for access to Rancho La Morita. Accommodations and fine company were provided by G. Axen and S. Augustin during resupply trips to Ensenada. Discussions with G. Axen, W. Bohrson, T. Dixon, P. Gans, C. Lewis, A. Martin Barajas, F. Suarez Vidal, and J. Stock contributed much to this work. Thorough formal reviews by K. Meisling, R. Sedlock, and M. Withjack improved the clarity and presentation of this manuscript. Stereonet and fault kinematic software were created by R. Allmendinger.

REFERENCES CITED

Allen, C. R., Silver, L. T., and Stechler, R. G., 1960, Agua Blanca fault—A major transverse structure of northern Baja California, Mexico: Geological Society of America Bulletin, v. 71, p. 457–482.

Angelier, J., Colletta, B., Chorowicz, J., Ortlieb, L., and Rangin, C., 1981, Fault tectonics of the Baja California peninsula and the opening of the Sea of Cortez, Mexico: Journal of Structural Geology, v. 3, p. 347–357.

Atwater, T. A., 1970, Implications of plate tectonic history of the northeast Pacific and western North America: Geological Society of America Bulletin, v. 81, p. 3513–3536.

Atwater, T. A., 1989, Plate tectonic history of the northeast Pacific and western North America, *in* Winterer, E. L., Hussong, D. M., and Decker, R. W., eds., The eastern Pacific Ocean and Hawaii: Geological Society of America, Geology of North America, v. N, p. 21–71.

Axen, G., 1995, Extensional segmentation of the Main Gulf Escarpment, Mexico and United States: Geology, v. 23, p. 515–518.

Boehm, M. C., 1984, An overview of the lithostratigraphy, biostratigraphy, and paleoenvironments of the late Neogene San Felipe marine sequence, Baja, California, Mexico, *in* Frizzell, V. A., Jr., ed., Geology of the Baja California peninsula: Society of Economic Paleontologists and Mineralogists Pacific Section, v. 39, p. 183–191.

Brown, L. G., 1978, Recent fault scarps along the eastern escarpment of the Sierra San Pedro Martir, Baja California [Master's thesis]: San Diego, California, San Diego State University, 108 p.

Bryant, B., 1986, Geology of the Sierra Santa Rosa Basin, Baja California, Mexico [Master's thesis]: San Diego, California, San Diego State University, 75 p.

Burchfiel, B. C., and Stewart, J. H., 1966, "Pull-apart" origin of the central segment of Death Valley, California: Geological Society of America Bulletin, v. 77, p. 439–442.

Coney, P. J., and Harms, T. A., 1984, Cordilleran metamorphic core complexes: Cenozoic extensional relics of Mesozoic compression: Geology, v. 12, p. 550–554.

Crippen, R. E., 1989a, Development of remote sensing techniques for the investigation of neotectonic activity, aastern Transverse Ranges and vicinity, southern California [Ph.D. thesis]: Santa Barbara, California, University of California, 304 p.

Crippen, R. E., 1989b, A simple spatial filtering routine for the cosmetic removal of scan-line noise from Landsat TM P-tape imagery: Photogrammetric Engineering and Remote Sensing, v. 55, p. 327–331.

Crippen, R. E., in press a, The iterative ratioing method of determining atmospheric corrections for scenes with rugged terrain: Photogrammetric Engineering and Remote Sensing.

Crippen, R. E., in press b, Image display of four components of spectral data: Remote Sensing of Environment.

Crowell, J., 1974, Origin of late Cenozoic basins in southern California, *in* Dickinson, W. R., ed., Tectonics and sedimentation: Society of Economic Paleontologists and Mineralogists Special Publication 22, p. 190–204.

Curray, J. R., and Moore, D. G., 1984, Geologic history of the mouth of the Gulf of California, *in* Crouch, J. K., and Bachman, S. B., eds., Tectonics and sedimentation along the California margin: Society of Economic Paleontologists and Mineralogists Pacific Section, v. 38, p. 17–36.

Curray, J. R., Moore, D. G., Kelts, D., and Einsele, G., 1982, Tectonics and geological history of the passive continental margin at the top of Baja California, *in* Curray, J. R. and Moore, D. G., et al., Initial reports of the Deep Sea Drilling Project: Washington D.C., U.S. Government Printing Office, p. 1089–1116.

DeMets, C., Gordon, R. G., Stein, S., and Argus, D. F., 1990, Current plate motions: Geophysical Journal International, v. 101, p. 425–478.

Dokka, R. K., and Merriam, R. H., 1982, Late Cenozoic extension of northeastern Baja California: Geological Society of America Bulletin, v. 93, p. 371–378.

Dorsey, R. J, and Burns, B., 1994, Regional stratigraphy, sedimentology, and tectonic significance of Oligocene–Miocene sedimentary and volcanic rocks, northern Baja California, Mexico: Sedimentary Geology, v. 88, p. 231–251.

Engebretsen, D. C., Cox, A., and Thompson, G. A., 1984, Correlation of plate motions with continental tectonics: Laramide to Basin-Range: Tectonics, v. 3, p. 115–120.

Engebretsen, D. C., Cox, A., and Gordon, R. G., 1985, Relative motions between oceanic and continental plates in the Pacific Basin: Geological Society of America Special Paper 206, 59 p.

Faulds, J. E., Geissman, J. W., and Mawer, C. K., 1990, Structural development of a major extensional accommodation zone in the Basin and Range Province, northwestern Arizona and southern Nevada; Implications for kinematic models of continental extension, *in* Wernicke, B. P., ed., Basin and Range extensional tectonics near the latitude of Las Vegas, Nevada: Geological Society of America Memoir 176, p. 37–76.

Fredrikson, G., 1971, Geology of the Huitis and La Mision quadrangles, northernmost Sinaloa, Mexico [Master's thesis]: Austin, University of Texas, 90 p.

Gastil, R. G., 1968, Fault systems in northern Baja California and their relation to the origin of the Gulf of California, *in* Proceedings, Conference on Geologic Problems of the San Andreas Fault System: Stanford, California, Stanford University Publications, Geological Sciences, v. 11, p. 283–286.

Gastil, R. G., and Krummenacher, D., 1977, Reconnaissance geology of coastal Sonora between Puerto Lobos and Bahia Kino: Geological Society of America Bulletin, v. 88, p. 189–198.

Gastil, R. G., and et al., 1974, Reconnaissance geologic map of coastal Sonora between Puerto Lobos and Bahia Kino: Geological Society of America Map and Chart Series MC-16.

Gastil, R. G., Phillips, R. P., and Allison, E. C., 1975, Reconnaissance geology of the State of Baja California: Geological Society of America Memoir 140, 170 p.

Gastil, R. G., Krummenacher, D., and Jensky, W. A., II, 1978, Reconnaissance geology of west-central Nayarit, Mexico: Geological Society of America Map and Chart Series MC-24.

Gastil, R. G., Krummenacher, D., and Minch, J., 1979, The record of Cenozoic volcanism around the Gulf of California: Geological Society of America Bulletin, v. 90, p. 839–837.

Gastil, R. G., Morgan, G. J., and Krummenacher, D., 1981, The tectonic history of peninsular California and adjacent Mexico, *in* The geotectonic development of California: [city], [publication], p. 284–305.

Gibbs, A. D., 1984, Structural evolution of extensional basin margins: Journal of the Geological Society of London, v. 141, p. 609–620.

Glazner, A. F. and Bartley, J. M., 1984, Timing and tectonic setting of Tertiary low-angle normal faulting and associated magmatism in the southwestern United States: Tectonics, v. 3, p. 385–396.

Hacker, B. R., 1993, Evolution of the northern Sierra Nevada metamorphic belt: Petrological, structural, and Ar/Ar constraints: Geological Society of America Bulletin, v. 105, p. 637–656.

Hausback, B. P., 1984, Cenozoic volcanic and tectonic evolution of Baja California Sur, Mexico, *in* Frizzell, V. A., Jr., ed., Geology of the Baja California peninsula: Los Angeles, Society of Economic Paleontologists and Mineralogists Pacific Section Publication, v. 39, p. 219–236.

Henry, C. D., 1989, Late Cenozoic Basin and Range structure in western Mexico adjacent to the Gulf of California: Geological Society of America Bulletin, v. 101, p. 1147–1156.

Henry, C. D., and Fredrikson, G., 1987, Geology of southern Sinaloa adjacent to the Gulf of California: Geological Society of America Map and Chart Series MCH063.

Henry, C. D., and Aranda-Gomez, J. J., 1992, The real southern Basin and Range: Mid- to late Cenozoic extension in Mexico: Geology, v. 20, p. 701–704.

Humphreys, E. D., and Weldon, R. J., II, 1991, Kinematic constraints on the rifting of Baja California, *in* Dauphin, J. P., and Simoneit, B. R. T., eds., The Gulf and Peninsular Province of the Californias: American Association of Petroleum Geologists Memoir 47, p. 217–229.

Ingersoll, R. V., 1982, Triple-junction instability as cause for late Cenozoic extension and fragmentation of the western United States: Geology, v. 10, p. 621–624.

Ingle, J. C., 1973, Neogene marine history of the Gulf of California: Geological Society of America Abstracts with Programs, v. 5, p. 62.

Ingle, J. C., 1974, Paleobathymetric history of Neogene marine sediments, northern Gulf of California, Geology of Peninsular California: Society of Economic Paleontologists and Mineralogists, and SEG Pacific Section, Guidebook for American Association of Petroleum Geologists, p. 121–138.

Ingle, J. C., 1984, Neogene marine stratigraphy of the Gulf of California: American Association of Petroleum Geologists Pacific Section, Annual Meeting, Program with Abstracts, p. 76–77.

Isaac, S., 1987, Geology and structure of the Yuha Desert between Ocotillo, California, U.S.A., and Laguna Salada, Baja California, Mexico [Master's thesis]: San Diego, California, San Diego State University, 165 p.

James, A. H., 1973, Structure and stratigraphy of the southern Sierra de Pintas, Baja California, Mexico [Master's thesis]: San Diego, California, San Diego State University.

Jensky, W. A., II, 1974, Reconnaissance geology and geochronology of the Bahia de Banderas area, Nayarit and Jalisco, Mexico [Master's thesis]: Santa Barbara, University of California, 80 p.

Karig, D. E., and Jensky, W. A., 1972, The proto–Gulf of California: Earth and Planetary Science Letters, v. 17, p. 169–174.

King, R. E., 1939, Geologic reconnaissance in the northern Sierra

Madre Occidental of Mexico: Geological Society of America Bulletin, v. 50, p. 1625–1722.
Larsen, P.-H., 1988, Relay structures in a Lower Permian basement-involved extension system, East Greenland: Journal of Structural Geology, v. 10, p. 3–8.
Larson, R. L., Menard, H. W., and Smith, S. M., 1968, Gulf of California: A result of ocean-floor spreading and transform faulting: Science, v. 161, p. 781–784.
Lee, J., and Miller, M. M., 1994, Middle Miocene extension in the Gulf Extensional Province, Baja California, Mexico: Geochronologic evidence from the southeastern Sierra Juarez: Geological Society of America Abstracts with Programs, v. 26, p. A65.
Lewis, C. J., 1994, Constraints on extension in the Gulf Extensional Province from the Sierra San Fermin, northeastern Baja California, Mexico [Ph.D. thesis]: Cambridge, Massachusetts, Harvard University, 361 p.
Lister, G. S., Etheridge, M. A., and Symonds, P. A., 1986, Detachment faulting and the evolution of passive continental margins: Geology, v. 14, p. 246–250.
Londsdale, P., 1991, Structural patterns of the Pacific floor offshore of peninsular California, *in* Dauphin, J. P., and Simoneit, B. R. T., eds., The Gulf and Peninsular Province of the Californias: American Association of Petroleum Geologists Memoir 47, p. 87–125.
Mammerickx, J., and Klitgord, K. D., 1982, Northern East Pacific Rise: evolution from 25 m.y.b.p. to the present: Journal of Geophysical Research, v. 87, p. 6751–6759.
Marrett, R., and Allmendinger, R. W., 1990, Kinematic analysis of fault-slip data: Journal of Structural Geology, v. 12, p. 973–986.
McCloy, C., and Ingle, J. C., 1982, Neogene foraminifera, stratigraphy, and depositional history of Isla Maria Madre: Evidence of early marine conditions in the Gulf of California: Geological Society of America Abstracts with Programs, v. 14, p. 213.
McCloy, C., 1984, Stratigraphy and depositional history of the San Jose del Cabo trough, Baja California Sur, Mexico: American Association of Petroleum Geologists Pacific Section, Annual Meeting, Program with Abstracts, p. 96.
McDowell, F. W., and Keizer, R. P., 1977, Timing of mid-Tertiary volcanism in the Sierra Madre Occidental between Durango City and Mazatlan, Mexico: Geological Society of America Bulletin, v. 88, p. 1479–1486.
McEldowney, R. C., 1970, Geology of the northern Sierra Pinta, Baja California Mexico [Master's thesis]: San Diego, California, San Diego State University, 74 p.
McFall, C. C., 1968, Reconnaissance geology of the Concepcion Bay area, Baja California, Mexico: Stanford University Publications, Geological Sciences, v. 10, p. 25.
McLean, H., 1988, Reconnaissance geologic map of the Loreto and part of the San Javier quadrangles, Baja California, Mexico: U.S. Geological Survey Map MF-2000.
Minch, J. A., 1979, The late Mesozoic-early Tertiary framework of continental sedimentation, northern Peninsular Ranges, Baja California, Mexico, *in* Abbott, P. L., ed., Eocene depositional systems: Bakersfield, California, Society of Economic Paleontologists and Mineralogists, Pacific Section, p. 43–68.
Moore, D. G., 1973, Plate-edge deformation and crustal growth of the Gulf of California since the late Pliocene: Science, v. 84, p. 1883–1906.
Moore, D. G., and Buffington, E. C., 1968, Transform faulting and growth of the Gulf of California since the late Pliocene: Science, v. 161, p. 1238–1241.
Moore, D. G., and Curray, J. R., 1982, Geologic and tectonic history of the Gulf of California, *in* Curry, J. R., Moore, D. G., et al., ed., Initial Reports of the Deep Sea Drilling Project: Washington D.C., U.S. Government Printing Office, p. 1279–1296.
Neuhaus, J. R., Cassidy, M., Krummenacher, D., and Gastil, R. G., 1988, Timing of protogulf extension and transtensional rifting through volcanic/sedimentary stratigraphy of SW Isla Tiburon, Gulf of California, Sonora, Mexico: Geological Society of America Abstracts with Programs, v. 20, p. 218.
Ortlieb, L., 1987, Neotectonique et variations du niveau marin au Quaternaire dans la region du Golfe de Californie, Mexique [Theses Etat thesis]: University Marseille II, France, 779 + 257 p.
Pollitz, P. P., 1988, Episodic North America and Pacific plate motions: Tectonics, v. 7, p. 711–726.
Rogers, M., 1970, Geology of Paso San Matias, Baja California, Mexico [senior report thesis]: San Diego, California, San Diego State University.
Sawlan, M. G., and Smith, J. G., 1984, Petrologic characteristics, age and tectonic setting of Neogene volcanic rocks in northern Baja California Sur, Mexico, *in* Frizzell, V. F., Jr, ed., Geology of the Baja California peninsula: Society of Economic Paleontologists and Mineralogists, Pacific Section, v. 39, p. 237–251.
Siem, M. E., and Gastil, R. G., 1994, Mid-Tertiary to Holocene extension associated with the development of the Sierra El Mayor metamorphic core complex, northeastern Baja California, Mexico, *in* McGill, S. F., and Ross, T. M., eds., Geological investigations of an active margin: San Bernardino, California, San Bernardino County Museum Association, Geological Society of America Cordilleran Section Guidebook, p. 107–119.
Smith, J. T., 1991, Cenozoic marine mollusks and paleography of the Gulf of California, *in* Dauphin, J. P., and Simoneit, B. R. T., eds., The Gulf and Peninsular Province of the Californias: American Association of Petroleum Geologists Memoir 47, p. 637–666.
Smith, J. T., Smith, J. G., Ingle, J. C., Gastil, R. G., Boehm, M. C., Roldan-Q., J., and Casey, R. E., 1985, Fossil and K-Ar age constraints on upper middle Miocene conglomerate, southwestern Isla Tiburon, Gulf of California: Geological Society of America Abstracts with Programs, v. 17, p. 409.
Spencer, J. E., and Normark, W. R., 1979, Tosco-Abreojos fault zone: A Neogene transform plate boundary within the Pacific margin of southern Baja California: Geology, v. 7, p. 554–557.
Stewart, J. A., 1978, Basin-range structure in western North America, a review, *in* Smith, R. B., and Eaton, G. P., eds., Cenozoic tectonics and regional geophysics of the western Cordillera: Geological Society of America Memoir 152, p. 1–13.
Stock, J. M., 1989, Sequence and geochronology of Miocene rocks adjacent to the Main Gulf Escarpment: Southern Valle Chico, Baja California Norte, Mexico: Geofisica Internacional, v. 28-5, p. 851–896.
Stock, J. M., and Hodges, K. V., 1989, Pre-Pliocene extension around the Gulf of California and the transfer of Baja California to the Pacific plate: Tectonics, v. 8, p. 99–115.
Stock, J. M., and Hodges, K. V., 1990, Miocene to Recent structural development of an extensional accommodation zone, northeastern Baja California, Mexico: Journal of Structural Geology, v. 12, p. 315–328.
Stock, J. M., and Lee, J., 1994, When do microplates in subduction zones leave a geological record?: Tectonics, v. 13, p. 1472–1487.
Stock, J. M., and Molnar, P., 1988, Uncertainties and implications of the Late Cretaceous and Tertiary positions of North America relative to the Farallon, Kula and Pacific plates: Tectonics, v. 7, p. 1339–1384.
Stone, K. A., Umhoefer, P. J., and Dorsey, R. J., 1994, Structural style and kinematics of the southeastern part of the Pliocene Loreto Basin, Baja California Sur, Mexico: Geological Society of America Abstracts with Programs, v. 26, p. 97.
Tron, V., and Brun, J.-P., 1991, Experiments on oblique rifting in brittle-ductile systems: Tectonophysics, v. 188, p. 71–84.
Umhoffer, P. J., and Dorsey, R. J., 1994, California Sur, Mexico, and evolution of the Gulf of California: Geology, v. 22, p. 649–652.
Wernicke, B. P., Christiansen, R. L., England, P. C., and Sonder, L. J., 1987, Tectonomagmatic evolution of Cenozoic extension in the North American Cordillera, *in* Coward, M. P., Dewey, J. F., and Hancock, P. L., eds., Continental extensional tectonics: Geological Society of America Special Paper 28, p. 203–221.
Wilson, I. F., and Rocha, V. S., 1955, Geology and mineral deposits of the Boleo copper district, Baja California, Mexico: U.S. Geological Survey Professional Paper 273, 134 p.
Wilson, I. F., and Veytia, M., 1949, Geology and manganese deposits of the Lucifer district, northwest of Santa Rosalia, Baja California, Mexico: U.S. Geological Survey Professional Paper 960-F, p. 177–233.
Withjack, M. O., and Jamison, W. R., 1986, Deformation produced by oblique rifting: Tectonophysics, v. 126, p. 99–124.

Manuscript Received by the Society October 7, 1994
Manuscript Accepted October 2, 1995

Printed in U.S.A.